J. Appl. Comput. Mech., xx(x) (2023) 1-15
DOI: 10.22055/jacm.2022.41704.3800

ISSN: 2383-4536
jacm.scu.ac.ir

Shahid Chamran University of Ahvaz

Journal of Applied and Computational Mechanics

Research Paper

A Novel Approach to Fully Nonlinear Mathematical Modeling of Tectonic Plates

Shahriar Dastjerdi[1], Mohammad Malikan[2], Bekir Akgöz[1], Ömer Civalek[1,3], Victor A. Eremeyev[2,4]

[1] Division of Mechanics, Civil Engineering Department, Akdeniz University, Antalya, 07058, Turkey, Emails: dastjerdi_shahriar@yahoo.com (S.D.), bekirakgoz@akdeniz.edu.tr (B.A.), ocivalek@akdeniz.edu.tr (Ö.C.)

[2] Department of Mechanics of Materials and Structures, Faculty of Civil and Environmental Engineering, Gdansk University of Technology, 80-233, Gdansk, Poland, Emails: mohammad.malikan@pg.edu.pl (M.M.), victo.eremeev@pg.edu.pl (V.A.E.)

[3] Department of Medical Research, China Medical University Hospital, China Medical University, Taichung 406, Taiwan, Email: civalek@yahoo.com

[4] DICAAR, Università degli Studi di Cagliari, Via Marengo, 2, 09123, Cagliari, Italy, Email: victor.eremeev@unica.it

Received August 24 2022; Revised September 30 2022; Accepted for publication October 04 2022.
Corresponding author: M. Malikan (mohammad.malikan@pg.edu.pl)

Abstract. The motion of the Earth's layers due to internal pressures is simulated in this research with an efficient mathematical model. The Earth, which revolves around its axis of rotation and is under internal pressure, will change the shape and displacement of the internal layers and tectonic plates. Applied mathematical models are based on a new approach to shell theory involving both two and three-dimensional approaches. It is the first time studying all necessary measures that increase the accuracy of the obtained results. These parameters are essential to perform a completely nonlinear analysis and consider the effects of the Earth's rotation around its axis. Unlike most modeling of nonlinear partial differential equations in applied mechanics that only considers nonlinear effects in a particular direction, the general nonlinear terms are considered in the present study, which increases the accuracy of the amount of displacement of the Earth's inner layers. Also, the fully nonlinear and dynamic differential equations are solved by a semi-analytical polynomial method which is an innovative and efficient method. Determining the amount of critical pressure at the fault location that will cause phenomena such as earthquakes is one of the useful results that can be obtained from the mathematical modeling in this research.

Keywords: Planet Earth, Tectonics plates, Nonlinear dynamic analysis, Semi-analytical polynomial method.

1. Introduction

Scientists think the Earth formed about the same time as the Sun and other planets about 4.6 billion years ago when the solar system and the giant gas orbiting cloud and dust, known as the Solar Nebula, came together. When the nebula collapsed due to gravity, it spun faster and became a flat disk. The majority of material due to gravitational force formed a huge spherical shape which is called the Sun. Other particles inside the disk collided and clung together to form larger objects, including the Earth. Scientists assume the Earth started as a waterless mass of rock. But in recent years, new analyzes of minerals trapped in ancient microscopic crystals show that liquid water existed on Earth, during the first 500 million years. The radioactive material in the rock and the increase in pressure in the depths of the Earth create enough heat to melt the planet's interior, causing some chemicals to come to the surface, and form water, while others turn into atmospheric gases.

Nowadays, it is found that oceans and the Earth's crust might have formed about 200 million years after the initial forming of the planet. As the Earth revolves around the Sun, it also rotates on an imaginary line called the axis, which runs from the North Pole to the South Pole. The Earth needs 23.934 hours to rotate on its axis and 365.26 days to orbit the Sun. The axis of rotation of the Earth is tilted relative to the plane of the zodiac (corresponding to the eclipse), which is an imaginary surface of the planet's orbit around the Sun. Earth's orbit is not a complete circle but is similar to the orbits of other planets, oval. Our planet is slightly closer to the Sun in early January and slightly away from the Sun in July, although these changes have very little effect on the warming and cooling of the Earth's axis.

Earth's core is approximately measured as 4400 miles (7081.11 km). Also, it is slightly larger than 50% of entire the Earth's diameter. The farthest core is 1400 miles (2253.08 km) in a molten state, while the inner core is solid. It is about four-fifths the size of Earth and is about 1600 miles (2574.95 km) in diameter. The core is responsible for the planet Earth's magnetic field which helps deflect harmful charged particles fired from the Sun. The Earth's mantle is settled above the core, and its thickness is about 1800 miles (2896.82 km). The mantle is not completely rigid and can flow slowly. The Earth's crust floats on the mantle like a piece of wood. The gentle movement of a rock in the mantle moves the continents back and forth, causing earthquakes, volcanoes, and mountain ranges. At the top of the mantle, the Earth has two types of crusts. The land of the continents is composed mostly of granite and other light silicate minerals, while the ocean floor is composed mostly of a dark, dense volcanic rock called basalt. The

Published online: October 14 2022

crust is on average about 25 miles (40.23 km) thick, although in some areas it can be thin and thick. The oceanic crust is usually only about 5 miles (8.05 km) thick. As we get closer to the Earth's core, the temperature gets warmer. At the bottom of the crust, the temperature rises to about 982.22°C and rises to about 1°C below the crust. Geologist assumes that the temperature of the Earth's outer core is around 3000 to 4300°C, and also the inner core temperature is considered 7000°C. This value is more than the Sun's outer surface temperature. The internal pressure of the Earth is relatively easy to estimate. The pressure of each point, below the sphere, is determined according to the thickness, and density of the upper rocks. As it is mentioned, the density of different layers can be obtained based on seismic wave data. This makes it possible to calculate the pressure as a function of depth. The pressure in the center of the Earth reaches more than 3.5 million times the atmospheric pressure on the Earth's surface. The temperature in the Earth's crust rises by about 30°C per kilometer deep. Of course, for deeper parts, this increase is slower. For example, at a depth of 2800 km, the temperature should have reached 8400°C, at which point the rocks can no longer be solid or even liquid. Therefore, the temperature of the mantle and core should be much lower than these values.

Navabi and Barati [1] modeled the magnetic field of Earth. They claimed that their study can help space missions. Some research has been conducted to model the Earth's pressure, inner core, and Earth's crust [2-4]. Wang et al. [5] have done an experience to determine collisional tectonics on early Earth. Recently, studies about tectonics on Earth have been done by researchers [6-10]. It can be seen that there is no research in which the movements of the Earth's layers are simulated as a mathematical model or it is not comprehensive and may only examine a specific subject in this field. Therefore, mathematical and mechanical models that have studied shell structures, especially spherical ones, can be used very effectively. In the following, previous research in this regard is summarized.

Pang et al. [11] investigated the free vibrational behavior of doubly-curved shells of revolution with arbitrary boundary conditions. They used Flügge's thin shell theory and the Rayleigh-Ritz method in the modeling and solution. Dastjerdi et al. [12-14] studied the bending and dynamic analysis of plate and shell structures in macro and nano sizes. They could propose a comprehensive model due to the mechanical point of view in their studies. They considered two and three-dimensional analyzes and also, and assumed a nonlinear strain field in all of their studies to obtain more accurate results, especially for large deformation analysis. Zeighampour and Beni [15] analyzed conical shells utilizing the couple stress theory. Dastjerdi and Akgöz [16] modeled a fullerene structure using a spherical geometric shape and found its static behavior under static uniform transverse loading. Pietraszkiewicz [17] investigated thermo-mechanics of shells using 3D laws of continuum thermo-mechanics. Geometrically nonlinear analysis of shell structures is investigated by using a flat triangular shell finite element [18] with the meshless method. Also, Dastjerdi et al. [19] studied the dynamic analysis of spherical gyroscopes with variable thicknesses made of functionally graded materials. They considered two independent rotation axes due to the simulation of gyroscopic effects. The dynamic investigations of shell structures were examined experimentally and for optimizing purposes [20, 21]. Lavrencic and Brank [22] comprehensively reviewed and compared many mixed and mixed-hybrid nonlinear shell finite element formulations to indicate those that are closest to the optimal one. Lee and Hodges [23] analyzed the mechanical behavior of laminated composite shells. Zhang et al. [24] studied a computational method for dynamic analysis of flexible sandwich plates. Experimental and analytical studies have been done by Li et al. [25] to determine the deformation and failure of a thin spherical structure under dynamic impact loading. Sharma and Panda [26] proposed a numerical scheme based on the higher-order shear deformation theory in conjunctions with coupled finite and boundary elements to examine the vibroacoustic responses of laminated composite sandwich curved shell panels under a harmonic point load. Eyvazian and his colleagues [27] studied the dynamic of reinforced nanocomposite shells exposed to a moving load. Fadida et al. [28] studied the static as well as dynamic shear-tension behavior of additively manufactured Ti6Al4V containing spherical and prolate voids. Serhat et al. [29] studied the dynamic analysis of doubly curved composite panels utilizing lamination coefficients and the spectral-Tchebychev technique. Li et al. [30] conducted research on the dynamic characteristics of saturated poroelastic media via Newmark finite element methods. Viana et al. [31] examined the nonlinear dynamic behavior of steel frames with the plastic zone technique via the Corotational approach. Huang et al. [32] presented a damping model for nonlinear dynamic investigation. The nonlinear dynamic analysis of laminated doubly curved panels subjected to thermal surroundings was presented by Li et al. [33]. Fu et al. [34] investigated dynamic analysis of porous FGM conical shells exposed to parametric excitation in thermal surroundings based on FSDT via generalized differential quadrature. Zhang et al. [35] studied the nonlinear dynamic characteristics of large-scale single-layer lattice domes. Also, some other dynamic analyses [36-42] were conducted recently. Monge et al. [43] studied the static and deformation behavior of doubly curved laminated composite shells under different types of loading conditions. Mellouli et al. [44] surveyed the free vibration response of FG carbon nanotube-reinforced shell structures on the basis of a modified Mindlin-Reissner theory and meshfree radial point interpolation method. Zhao et al. [45] perused dynamical analysis of hyperelastic spherical shells subjected to dynamic loads with structural damping. The analytical solution of stress distribution of FG hollow cylinder/spherical pressure vessel was presented and compared with the numerical and classical solutions by Xie et al. [46]. Yi et al. [47] investigated large amplitude and nonlinear natural frequencies of functionally graded small-scale shells with pores inside the composite. Also, some other mechanical analyses of related topics can be found in [48-59].

After a literature survey, it appears that no study has yet been carried out to provide a comprehensive mechanical and mathematical model to simulate the movements of the Earth's layers that are subjected to internal pressures. The study of the behavior of the Earth's layers is often the result of experimental works, which are very costly and sometimes impossible due to the very high temperatures and pressures in the Earth's inner layers. Therefore, in this study, the planet Earth is theoretically and mathematically modeled by the geometric shape of a sphere, in which different inner layers have different thicknesses. Two-dimensional and three-dimensional shell theories are employed and the governing partial differential equations of the model are derived. Attempts are made to consider most of the prevailing conditions, such as the Earth's rotation around its axis (which rotates one full revolution every 24 hours) and the pressure gradient in the internal layers. Semi-analytical polynomial method (SAPM) is applied to solve the resulting dynamic equations. The important point in this modeling is completely nonlinear analysis in all the main three independent directions of the problem. In other words, in addition to the radial direction, there are nonlinear parameters in both latitude and longitude to have the highest possible accuracy in the results. This research can provide relevant information on the deformation of the Earth's layers under internal pressures to researchers working in this field. Also, the presented nonlinear governing differential equations are comprehensive equations that are able to give desirable results by changing any parameters.

2. Structure of the Earth's Layers

Figure 1 shows the schematic view of the planet Earth considering its sub-layers. The Earth has two bevels in the North and South Poles, which are created due to the rotation of the Earth (revolution of the Earth around its central axis). The axis of rotation of the Earth is angular with respect to its orbit around the sun (axial tilt about 23.4°). As mentioned earlier, this aspect causes the seasons to occur due to differences in the angle of sunlight to the Earth. It is also observed that due to this axial tilt, the seasons in the Northern hemisphere are opposite to the Southern. For example, if it is summer in the Northern hemisphere, the inhabitants

of the Southern hemisphere will experience winter. As a result, in the equator regions due to the constant angle of sunlight during the year, the seasons will not be changed significantly and the temperature difference is small. Also, the five inner layers of the Earth are shown and determined in Figure 1. The average radius of the Earth is shown as R_E which equals 6371 kilometers (approximately).

It is observed that the outermost layer of the Earth is its crust, which is made of minerals and there is life in this layer. The mantle itself consists of two sub-layers, the upper mantle, and the lower mantle, and is the largest layer of the Earth. This layer is made of very soft and dense semi-solid rocks that are mostly composed of iron and magnesium. The layers of the Earth's crust are constantly moving. The movements of tectonics plates cause continental drift, according to which the lithosphere which itself consists of 7 or 8 main plates is constantly moving, and due to the collision of these plates' phenomena such as earthquakes, subsequent tectonic folding, the formation of mountains and geological depression will occur. The 7 main plate tectonics can be categorized as follows: 1- Pacific plate 2- North American plate 3- South American plate 4- Australian plate 5- African plate 6- Indian plate 7- Antarctic plate

The Earth's outer core is made of molten metals, iron, and nickel as well as sulfur. This layer controls the Earth's magnetic field. The inner core, which is under considerable pressure is solid and made of iron. The temperature of the inner core is about 6000°C, which is very high and about the temperature of the sun's surface. The pressure in this area is about 310 GPa.

The shape of the Earth has always changed over time. For example, about 270 million years ago, there was a supercontinent called Pangea, which included all existing continents. Over time, this vast continent has disintegrated due to tectonics and formed new continents.

The oceanic and continental crusts form the Earth's crust. The oceanic crust is heavier than the continental crust and sinks very slowly beneath the continental crust. The graph of pressure (q_r in GPa, r, and R_E in km) due to the depth from the surface of the Earth (h) can be seen in Figure 2. The main equation of internal pressure on the planet Earth will be derived as follow [60, 61]:

$$\begin{cases} \rho(r) = 11200\left(1 - 0.76\left(1 - \dfrac{r}{R_E}\right)^2\right) = 11200 - 8512\left(1 - \dfrac{r}{R_E}\right)^2 \\ g(r) = \dfrac{4}{3}\pi G\rho(r)(R_E - r) \end{cases} \tag{1}$$

$$q_r = 10^{-3}\left(\int_0^r \rho(r)g(r)dr\right) \tag{2}$$

In the above equations, $\rho(r)$, $g(r)$, and G are the density, gravitational acceleration, and the universal gravitational constant respectively (G = 6.6740831×10^{-11} m^3/kgS^2, π = 3.1415926535).

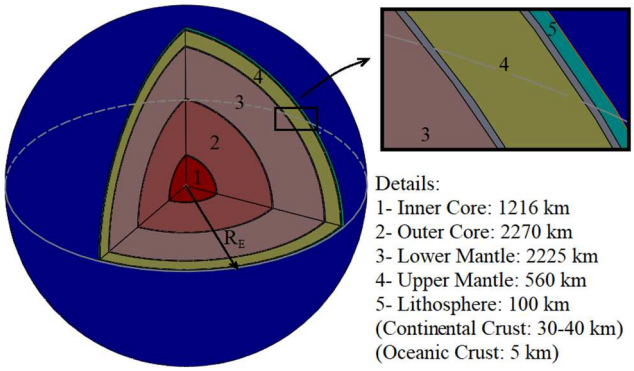

Fig. 1. Schematic view of the planet Earth and its five distinctive layers.

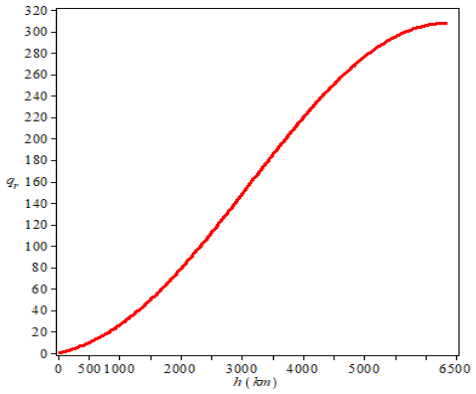

Fig. 2. Variations of the internal Earth pressure (q_r in GPa) versus the amount of depth (h).

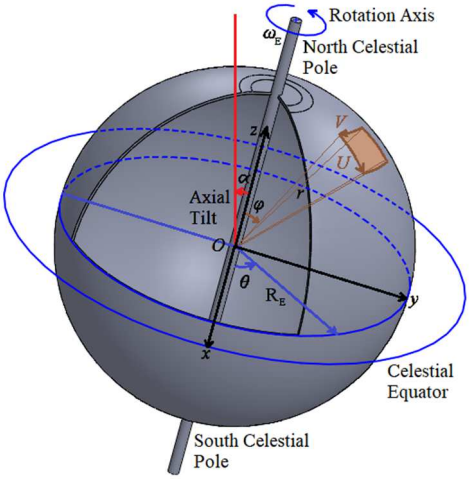

Fig. 3. Geographic view of the planet Earth and the applied spherical coordinates system.

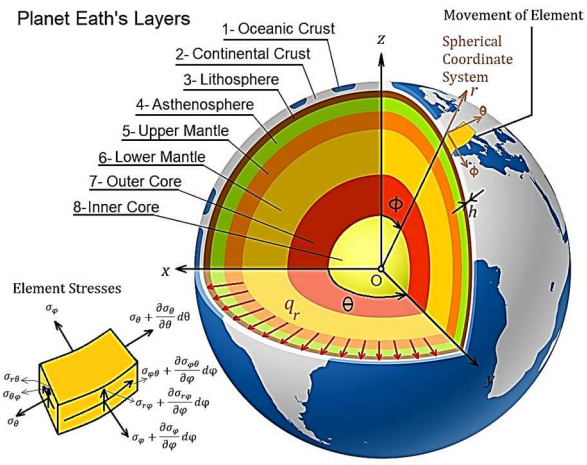

Fig. 4. Schematic representation of the Earth's layers and element stresses.

3. Mathematical Modeling of the Earth

A schematic representation of the Earth's layers and element stresses in a spherical coordinates system is illustrated in Figures 3 and 4. As mentioned in the previous section, the Earth can be simulated by a sphere with a radius of 6371 km. The Earth also rotates around an axis that extends from the North Pole to the South. The rotational speed of the Earth (ω_E) can be estimated once every 23 hours, 56 minutes, and 4 seconds and this rotational speed is constant. Therefore, it does not change significantly over time, in other words, $\frac{\partial \omega_E}{\partial t} = \dot{\theta} = 0$. The location of a person on the surface of the Earth can be determined according to Figure 3 based on the two angles θ and φ (in practice these two angles are longitude and latitude).

The difference in the height on the Earth's surface is ignored, in other words, the Earth's surface is assumed to be smooth. The assumption is not far from the truth because if the altitude at the ocean level is based on zero, the difference between the maximum height (Mount Everest) and the deepest trench in the oceans (Challenger deep in Mariana trench) will be about 20 km, which is compared to the average radius of the Earth is about 0.3% and can be neglected. The base pressure for the calculations is the pressure applied below the surface of the Earth's crust at a depth of 75 km, which will cause tectonics movements of the layers. Also, the applied pressure and movement of the ground plates cause wrinkles on the ground surface. Therefore, according to Figures 3 and 4, q_r is applied pressure uniformly throughout the Earth's crust to its lower surface. Also, to increase the accuracy of simulating the two pressures q_θ and q_φ in the two directions θ and φ under the crust are considered (which causes transverse and longitudinal displacement of the layers). To better understand the effect of the applied loads, the intended element on the surface of the sphere is magnified. The relationships between the Spherical coordinate system and the Cartesian coordinate system can be formulated as follows [62]:

$$\begin{cases} x = r\sin\varphi\cos\theta \\ y = r\sin\varphi\sin\theta \\ z = r\cos\varphi \end{cases} \tag{3}$$

According to the above equations, the changes in the Spherical coordinate system based on the variables in the Cartesian coordinate system will be written as the following equations:

$$\begin{cases} \left(\frac{\partial}{\partial r}\right) = \sin\varphi\cos\theta\left(\frac{\partial}{\partial x}\right) + \sin\varphi\sin\theta\left(\frac{\partial}{\partial y}\right) + \cos\varphi\left(\frac{\partial}{\partial z}\right) \\ \left(\frac{\partial}{\partial \varphi}\right) = \frac{1}{r}\cos\varphi\cos\theta\left(\frac{\partial}{\partial x}\right) + \frac{1}{r}\cos\varphi\sin\theta\left(\frac{\partial}{\partial y}\right) - \frac{1}{r}\sin\varphi\left(\frac{\partial}{\partial z}\right) \\ \left(\frac{\partial}{\partial \theta}\right) = \frac{1}{r\sin\varphi}\sin\theta\left(\frac{\partial}{\partial x}\right) + \frac{1}{r\sin\varphi}\cos\theta\left(\frac{\partial}{\partial y}\right) \end{cases} \tag{4}$$

Therefore, the gradient vector of changes in the spherical coordinate system ($\nabla_{\text{Spherical}}$) is introduced based on the above equations as follows (R is the sphere radius) [62]:

$$\vec{\nabla}_{\text{Spherical}} = \left[\frac{\partial}{\partial r}\hat{e}_r \quad \frac{1}{R}\frac{\partial}{\partial \varphi}\hat{e}_\varphi \quad \frac{1}{R\sin\varphi}\frac{\partial}{\partial \theta}\hat{e}_\theta\right] \tag{5}$$

If the displacement vector of a hypothetical point on the surface of the sphere is assumed to be $\vec{U} = U_r\hat{e}_r + U_\theta\hat{e}_\theta + U_\varphi\hat{e}_\varphi$, the strain components can be obtained in the spherical coordinate system with respect to the fundamental equation of the strain tensor as follow [62]:

$$\vec{\varepsilon} = \frac{1}{2}\left[\nabla\vec{U} + \nabla\vec{U}^T + \nabla\vec{U}\cdot\nabla\vec{U}^T\right] \tag{6}$$

The above equation can be applied in any coordinate system. Also, $\vec{\varepsilon}$ is the strain tensor, ∇ is the gradient in the assumed coordinate system and $\vec{U}$ is the displacement vector. T symbol refers to the matrix transpose. According to the mathematical Equation (6) and the definition of the dyadic multiplication of the components of the assumed coordinate system (which here are the components of the spherical coordinate system $\hat{e}_r, \hat{e}_\theta$ and $\hat{e}_\varphi$, the components of the strain tensor can be obtained (the tensor is a symmetric 3×3 matrix). α_{Th} and ΔT are the thermal expansion coefficient and temperature difference, respectively [62]:

$$\nabla\vec{U} = \left[\frac{\partial}{\partial r}\hat{e}_r \quad \frac{1}{R}\frac{\partial}{\partial \varphi}\hat{e}_\varphi \quad \frac{1}{R\sin\varphi}\frac{\partial}{\partial \theta}\hat{e}_\theta\right]\begin{bmatrix} U_r\hat{e}_r \\ U_\varphi\hat{e}_\varphi \\ U_\theta\hat{e}_\theta \end{bmatrix} = \begin{bmatrix} \frac{\partial U_r}{\partial r} & \frac{\partial U_\varphi}{\partial r} & \frac{\partial U_\theta}{\partial r} \\ \frac{1}{R}\left(\frac{\partial U_r}{\partial \varphi} - U_\varphi\right) & \frac{1}{R}\left(\frac{\partial U_\varphi}{\partial \varphi} + U_r\right) & \frac{1}{R}\frac{\partial U_\theta}{\partial \varphi} \\ \frac{1}{R}\left(\frac{1}{\sin\varphi}\frac{\partial U_r}{\partial \theta} - U_\theta\right) & \frac{1}{R}\left(\frac{1}{\sin\varphi}\frac{\partial U_\varphi}{\partial \theta} - \cot\varphi\, U_\theta\right) & \frac{1}{R}\left(U_r + \cot\varphi\, U_\varphi + \frac{1}{\sin\varphi}\frac{\partial U_\theta}{\partial \theta}\right) \end{bmatrix} \tag{7}$$

$$\nabla\vec{U}^T = \begin{bmatrix} \frac{\partial U_r}{\partial r} & \frac{1}{R}\left(\frac{\partial U_r}{\partial \varphi} - U_\varphi\right) & \frac{1}{R}\left(\frac{1}{\sin\varphi}\frac{\partial U_r}{\partial \theta} - U_\theta\right) \\ \frac{\partial U_\varphi}{\partial r} & \frac{1}{R}\left(\frac{\partial U_\varphi}{\partial \varphi} + U_r\right) & \frac{1}{R}\left(\frac{1}{\sin\varphi}\frac{\partial U_\varphi}{\partial \theta} - \cot\varphi\, U_\theta\right) \\ \frac{\partial U_\theta}{\partial r} & \frac{1}{R}\frac{\partial U_\theta}{\partial \varphi} & \frac{1}{R}\left(U_r + \cot\varphi\, U_\varphi + \frac{1}{\sin\varphi}\frac{\partial U_\theta}{\partial \theta}\right) \end{bmatrix} \tag{8}$$

$$\vec{\varepsilon}_{ij} = \begin{bmatrix} \varepsilon_{rr} & \varepsilon_{r\varphi} & \varepsilon_{r\theta} \\ \varepsilon_{\varphi r} & \varepsilon_{\varphi\varphi} & \varepsilon_{\varphi\theta} \\ \varepsilon_{\theta r} & \varepsilon_{\theta\varphi} & \varepsilon_{\theta\theta} \end{bmatrix} - (\alpha_{Th}\Delta T)\begin{bmatrix} 1 & 0 & 0 \\ 0 & 1 & 0 \\ 0 & 0 & 1 \end{bmatrix} \tag{9}$$

$$\varepsilon_{rr} = \left(\frac{\partial U_r}{\partial r}\right) + \frac{1}{2}\left(\left(\frac{\partial U_r}{\partial r}\right)^2 + \left(\frac{\partial U_\varphi}{\partial r}\right)^2 + \left(\frac{\partial U_\theta}{\partial r}\right)^2\right) - (\alpha_{Th}\Delta T) \tag{10}$$

$$2\varepsilon_{r\varphi} = 2\varepsilon_{\varphi r} = \frac{\partial U_\varphi}{\partial r} + \frac{1}{R}\left(\frac{\partial U_r}{\partial \varphi} - U_\varphi\right) + \frac{1}{R}\left(\left(\frac{\partial U_r}{\partial r}\right)\left(\frac{\partial U_r}{\partial \varphi} - U_\varphi\right) + \left(\frac{\partial U_\varphi}{\partial r}\right)\left(\frac{\partial U_\varphi}{\partial \varphi} + U_r\right) + \left(\frac{\partial U_\theta}{\partial r}\right)\left(\frac{\partial U_\theta}{\partial \varphi}\right)\right) \tag{11}$$

$$2\varepsilon_{r\theta}=2\varepsilon_{\theta r}=\frac{\partial U_\theta}{\partial r}+\frac{1}{R}\left(\frac{1}{\sin\varphi}\frac{\partial U_r}{\partial\theta}-U_\theta\right)+\frac{1}{R}\left(\left(\frac{\partial U_r}{\partial r}\right)\left(\frac{1}{\sin\varphi}\frac{\partial U_r}{\partial\theta}-U_\theta\right)+\left(\frac{\partial U_\varphi}{\partial r}\right)\left(\frac{1}{\sin\varphi}\frac{\partial U_\varphi}{\partial\theta}-\cot\varphi\,U_\theta\right)+\left(\frac{\partial U_\theta}{\partial r}\right)\left(U_r+\cot\varphi\,U_\varphi+\frac{1}{\sin\varphi}\frac{\partial U_\theta}{\partial\theta}\right)\right) \tag{12}$$

$$\varepsilon_{\varphi\varphi}=\frac{1}{R}\left(\frac{\partial U_\varphi}{\partial\varphi}+U_r\right)+\frac{1}{2R^2}\left(\left(\frac{\partial U_r}{\partial\varphi}-U_\varphi\right)^2+\left(\frac{\partial U_\varphi}{\partial\varphi}+U_r\right)^2+\left(\frac{\partial U_\theta}{\partial\varphi}\right)^2\right)-(\alpha_{Th}\Delta T) \tag{13}$$

$$2\varepsilon_{\varphi\theta}=2\varepsilon_{\theta\varphi}=\frac{1}{R}\left(\frac{\partial U_\theta}{\partial\varphi}+\frac{1}{\sin\varphi}\frac{\partial U_\varphi}{\partial\theta}-\cot\varphi\,U_\theta\right)+\frac{1}{R^2}\left(\left(\frac{\partial U_r}{\partial\varphi}-U_\varphi\right)\left(\frac{1}{\sin\varphi}\frac{\partial U_r}{\partial\theta}-U_\theta\right)+\left(\frac{\partial U_\varphi}{\partial\varphi}+U_r\right)\left(\frac{1}{\sin\varphi}\frac{\partial U_\varphi}{\partial\theta}-\cot\varphi\,U_\theta\right)+\left(\frac{\partial U_\theta}{\partial\varphi}\right)\left(U_r+\cot\varphi\,U_\varphi+\frac{1}{\sin\varphi}\frac{\partial U_\theta}{\partial\theta}\right)\right) \tag{14}$$

$$\varepsilon_{\theta\theta}=\frac{1}{R}\left(U_r+\cot\varphi\,U_\varphi+\frac{1}{\sin\varphi}\frac{\partial U_\theta}{\partial\theta}\right)+\frac{1}{2R^2}\left(\left(\frac{1}{\sin\varphi}\frac{\partial U_r}{\partial\theta}-U_\theta\right)^2+\frac{1}{R}\left(\frac{1}{\sin\varphi}\frac{\partial U_\varphi}{\partial\theta}-\cot\varphi\,U_\theta\right)^2+\left(U_r+\cot\varphi\,U_\varphi+\frac{1}{\sin\varphi}\frac{\partial U_\theta}{\partial\theta}\right)^2\right)-(\alpha_{Th}\Delta T) \tag{15}$$

A noteworthy point in the strain components is the nonlinear terms. In the nonlinear modeling of plates and shells, the von Kármán strain field is often used, in which the nonlinear effects of displacements in the direction of the applied load to the structure are considered, and the effect of other nonlinear parameters are omitted. However, in this study, due to the special importance of the results in the other directions (except the loading direction) that cause the movement of the inner layers and tectonic plates of the Earth, the effects of nonlinear terms in the mentioned directions (here θ and φ) have not been neglected. As in most studies, which consider the load on the structure only in one direction and perpendicular to the structure, in this research there is a load in all three main directions r, θ, and φ. Therefore, it is expected that due to non-linear parameters in all major directions (r, θ, and φ), the results of mathematical simulation have high and appropriate accuracy.

The obtained strain field ($\vec{\varepsilon}$) is in a general form. In other words, the functions U_r, U_θ, and U_φ are independent functions consisting of three variables r, θ, and φ. One of the strengths of the strain field introduced in this research is the generality and definition of strain in a general form. Therefore, any desired function can be considered for displacement functions U_r, U_θ, and U_φ. The choice of displacement functions will determine the type of theory as well as the number of final obtained equations. Various theories have been proposed by mechanical scientists in this regard, which in general can be divided into two categories: 1. Theories that ignore strain changes in the thickness of the structure ($\varepsilon_{thickness}=0$). 2. Theories that do not assume the amount of strain in the direction of thickness to be zero ($\varepsilon_{thickness}\neq 0$) and take these changes into account in the calculations.

In general, the first category theories are used for structures with a thickness considerably less than the other sizes of the structure. For example, in the spherical structure, the ratio of the radius R to the thickness *h* is important, and usually, if this ratio is R/*h* > 10, the use of the first category theories provides good results with insignificant errors. However, if the R/*h* ratio is less than 10, the amount of strain in the thickness direction is significant, and ignoring it causes serious errors in the results, and therefore the second category theories should be used. It should be noted that the so-called theories in which $\varepsilon_{thickness}\neq 0$, are called three-dimensional theories. They are divided into two categories of exact 3D theories and quasi-3D theories. Formulating and solving the obtained equations based on the second category theories is much more difficult and complex than the first one. Therefore, it is necessary to determine the R/*h* value of the problem in what interval it is in, and if this ratio has a large value, one can use the first category theories to avoid complex and difficult calculations that are very time-consuming and sometimes unsolvable (since the obtained equations are also completely nonlinear).

In this study, the thickness of the Earth's structure is considered around its crust, which is 75 km. Given that the average radius of the Earth is R = 6371 km, so the ratio R/*h* is bigger than 10. As a result, the first category theories can be used with complete confidence.

The strain field used in this study to obtain the governing equations is based on the first-order shear deformation theory (FSDT). For the hypotheses considered in this study, the FSDT displacement field provides good results. The basic equations of FSDT theory for three displacements U_r, U_θ, and U_φ will be introduced as the following equations (t refers to the time variable) [16]:

$$\begin{cases}U_\varphi(r,\varphi,\theta,t)=u_0(\varphi,\theta,t)+r.\psi_1(\varphi,\theta,t)\\U_\theta(r,\varphi,\theta,t)=v_0(\varphi,\theta,t)+r.\psi_2(\varphi,\theta,t)\\U_r(r,\varphi,\theta,t)=w_0(\varphi,\theta,t)\end{cases} \tag{16}$$

Because the internal pressure of the Earth is assumed to be constant in the two assumed directions r, and φ (internal pressure in the θ-direction is neglected), and also because the geometry of the problem is considered to be a complete sphere, the changes in the θ-direction are constant and also because of the axial symmetry then U_θ will be zero. Boundary conditions at the North and South Poles are considered around the axis of the rotation. φ at the North and South Poles will be assumed to be very small. For example, φ_1= 5°, φ_2= 175° are considered and it is assumed that in these two angles there are clamped boundary conditions around the rotation axis. According to the given explanations, the equations of the displacement field will be rewritten as the following equations:

$$\begin{cases}U_\varphi(r,\varphi,t)=u_0(\varphi,t)+r.\psi_1(\varphi,t)\\U_\theta(r,\varphi,t)=0\\U_r(r,\varphi,t)=w_0(\varphi,t)\end{cases} \tag{17}$$

It is observed that the number of variables of U_i, $i=r$, and φ functions will change from three r, φ, and t variables to two φ and t variables. Because of presenting the time into functions (considering the revolution of the Earth around its rotation axes), a completely dynamic analysis is obtained. Consequently, the simulation will be as much as possible compatible with reality.

Now, by applying Equation (17) to the introduced strain field (Eqs. (10)-(15)), the nonlinear strain tensor components can be rewritten as the following relations:

$$\varepsilon_{rr}=\frac{1}{2}(\psi_1)^2-(\alpha_{Th}\Delta T) \tag{18}$$

$$2\varepsilon_{r\varphi}=2\varepsilon_{\varphi r}=\psi_1+\frac{1}{R}\left(\frac{\partial w_0}{\partial\varphi}-u_0-r\psi_1\right)+\frac{\psi_1}{R}\left(\frac{\partial u_0}{\partial\varphi}+r\frac{\partial\psi_1}{\partial\varphi}+w_0\right) \tag{19}$$

$$2\varepsilon_{r\theta} = 2\varepsilon_{\theta r} = 0 \tag{20}$$

$$\varepsilon_{\varphi\varphi} = \tfrac{1}{R}\left(\tfrac{\partial u_0}{\partial\varphi} + r\tfrac{\partial\psi_1}{\partial\varphi} + w_0\right) + \tfrac{1}{2R^2}\left(\left(\tfrac{\partial w_0}{\partial\varphi} - u_0 - r\psi_1\right)^2 + \left(\tfrac{\partial u_0}{\partial\varphi} + r\tfrac{\partial\psi_1}{\partial\varphi} + w_0\right)^2\right) - (\alpha_{Th}\Delta T) \tag{21}$$

$$2\varepsilon_{\varphi\theta} = 2\varepsilon_{\theta\varphi} = 0 \tag{22}$$

$$\varepsilon_{\theta\theta} = \frac{1}{R}\left(w_0 + \cot\varphi\,(u_0 + r\psi_1)\right) + \frac{1}{2R^2}\left(w_0 + \cot\varphi\,(u_0 + r\psi_1)\right)^2 - (\alpha_{Th}\Delta T) \tag{23}$$

4. Principle of Stationary Potential Energy

The principle of stationary potential energy has been used to obtain the governing equations due to the internal pressure under the Earth's crust that rotates around the axis of rotation. The main equation of this principle is the following equation, which consists of changes in strain energy δU_ε, changes in kinetic energy δU_k, and changes in work done by external forces (here due to the internal pressure of the Earth on its crust which is q_r) which are shown with δU_q and also the energy of centrifugal forces on the analysis δU_c. The summation of the mentioned energy variations ($\delta\Pi$) must be equal to zero [19]:

$$\delta\Pi = \delta U_\varepsilon + \delta U_k + \delta U_q + \delta U_c = 0 \tag{24}$$

$$\delta U_\varepsilon = \int_0^t \left(\iiint_V (\sigma_{rr}\delta\varepsilon_{rr} + \sigma_{\varphi\varphi}\delta\varepsilon_{\varphi\varphi} + \sigma_{\theta\theta}\delta\varepsilon_{\theta\theta} + 2\sigma_{r\varphi}\delta\varepsilon_{r\varphi})R^2\sin\varphi\, dr d\varphi d\theta\right) dt \tag{25}$$

$$\delta U_k = -\frac{\delta}{2}\int_0^t \left(\iiint_V \rho\left(\left(\frac{\partial U_r}{\partial t}\right)^2 + \left(\frac{\partial U_\varphi}{\partial t}\right)^2\right) dV\right) dt \tag{26}$$

$$\delta U_q = \int_0^t \left(-\iint_A \left(q_r(\delta w_0) + q_\varphi(\delta u_0 + r\delta\psi_1)\right) dA\right) dt \qquad (dA = R^2\sin\varphi\, d\varphi d\theta) \tag{27}$$

$$\delta U_c = -\int_0^t \left(\iiint_V \rho(a_r\delta w_0 + a_\varphi\delta u_0 + a_\varphi r\delta\psi_1) dV\right) dt \tag{28}$$

In Equation (28), a_r and a_φ are the radial and lateral accelerations respectively. According to the spherical coordinate system, the mentioned accelerations are formulated as the following equations. The rotational speed of the Earth is $\dot\theta = \frac{\partial\theta}{\partial t} = \omega_E$ and is considered to be constant. Consequently, the angular acceleration of the Earth is set to zero ($\ddot\theta = \frac{\partial^2\theta}{\partial t^2} = 0$) [19, 62]:

$$\begin{cases} a_r = R\omega_E^2\sin^2\varphi \\ a_\varphi = -R\omega_E^2\sin\varphi\cos\varphi \end{cases} \tag{29}$$

After substituting strain components into Equation (25) and expansion of Equations (26) and (28), the below equations are reformulated. It is noted that ρ is the average density of the material [19, 62]:

$$\begin{gathered} \delta U_k = -\int_0^t \left(\iiint_V \rho\left(\left(\tfrac{\partial U_\varphi}{\partial t}\tfrac{\partial\delta U_\varphi}{\partial t}\right) + \left(\tfrac{\partial U_r}{\partial t}\tfrac{\partial\delta U_r}{\partial t}\right)\right) dV\right) dt = -\int_0^t \left(\iiint_V \rho\left(\left(\tfrac{\partial u_0}{\partial t} + r\tfrac{\partial\psi_1}{\partial t}\right)\left(\tfrac{\partial\delta u_0}{\partial t} + r\tfrac{\partial\delta\psi_1}{\partial t}\right) + \left(\tfrac{\partial w_0}{\partial t}\tfrac{\partial\delta w_0}{\partial t}\right)\right) dV\right) dt = \\ -\int_0^t \left(\iint_A \left(I_1\left(\tfrac{\partial u_0}{\partial t}\tfrac{\partial\delta u_0}{\partial t}\right) + I_2\left(\tfrac{\partial u_0}{\partial t}\tfrac{\partial\delta\psi_1}{\partial t} + \tfrac{\partial\psi_1}{\partial t}\tfrac{\partial\delta u_0}{\partial t}\right) + I_3\left(\tfrac{\partial\psi_1}{\partial t}\tfrac{\partial\delta\psi_1}{\partial t}\right) + I_1\left(\tfrac{\partial w_0}{\partial t}\tfrac{\partial\delta w_0}{\partial t}\right)\right) R^2\sin\varphi\, d\varphi d\theta\right) dt \quad (I_1, I_2, I_3) = \int_{-\frac{h}{2}}^{\frac{h}{2}} \rho(1, r, r^2) dr \end{gathered} \tag{30}$$

$$\begin{gathered} \delta U_\varepsilon = \int_0^t \left(\int_{\theta_1}^{\theta_2}\int_{\varphi_1}^{\varphi_2}\int_{-\frac{h}{2}}^{\frac{h}{2}} \left(\sigma_{rr}(\psi_1\delta\psi_1) + \sigma_{r\varphi}\left(\delta\psi_1 + \tfrac{1}{R}\left(\tfrac{\partial\delta w_0}{\partial\varphi} - \delta u_0 - r\delta\psi_1\right) + \tfrac{1}{R}\left(\left(\delta\psi_1\tfrac{\partial u_0}{\partial\varphi} + \psi_1\tfrac{\partial\delta u_0}{\partial\varphi}\right) + r\left(\delta\psi_1\tfrac{\partial\psi_1}{\partial\varphi} + \psi_1\tfrac{\partial\delta\psi_1}{\partial\varphi}\right) + \right.\right.\right.\right. \\ \left.\left.\left.\left.(\delta\psi_1 w_0 + \psi_1\delta w_0)\right)\right) + \sigma_{\varphi\varphi}\left(\tfrac{1}{R}\left(\left(\tfrac{\partial\delta u_0}{\partial\varphi} + r\tfrac{\partial\delta\psi_1}{\partial\varphi} + \delta w_0\right) + \tfrac{1}{R}\left(\left(\tfrac{\partial\delta w_0}{\partial\varphi}\right)\left(\tfrac{\partial w_0}{\partial\varphi}\right) + u_0\delta u_0 + r^2\psi_1\delta\psi_1 - \delta u_0\left(\tfrac{\partial w_0}{\partial\varphi}\right) - u_0\left(\tfrac{\partial\delta w_0}{\partial\varphi}\right) - \right.\right.\right. \\ r\left(\delta\psi_1\left(\tfrac{\partial w_0}{\partial\varphi}\right) + \psi_1\left(\tfrac{\partial\delta w_0}{\partial\varphi}\right)\right) + r(\delta u_0\psi_1 + u_0\delta\psi_1) + \left(\tfrac{\partial\delta u_0}{\partial\varphi}\right)\left(\tfrac{\partial u_0}{\partial\varphi}\right) + r^2\left(\tfrac{\partial\delta\psi_1}{\partial\varphi}\right)\left(\tfrac{\partial\psi_1}{\partial\varphi}\right) + w_0\delta w_0 + r\left(\left(\tfrac{\partial\delta u_0}{\partial\varphi}\right)\left(\tfrac{\partial\psi_1}{\partial\varphi}\right) + \left(\tfrac{\partial u_0}{\partial\varphi}\right)\left(\tfrac{\partial\delta\psi_1}{\partial\varphi}\right)\right) + \\ \left.\left.\left.\left(\delta w_0\left(\tfrac{\partial u_0}{\partial\varphi}\right) + w_0\left(\tfrac{\partial\delta u_0}{\partial\varphi}\right)\right) + r\left(\delta w_0\left(\tfrac{\partial\psi_1}{\partial\varphi}\right) + w_0\left(\tfrac{\partial\delta\psi_1}{\partial\varphi}\right)\right)\right)\right)\right) + \sigma_{\theta\theta}\left(\tfrac{1}{R}\left((\delta w_0 + cot\,\varphi\,(\delta u_0 + r\delta\psi_1)) + \tfrac{1}{R}\left(w_0\delta w_0 + cot^2\,\varphi\, u_0\delta u_0 + \right.\right.\right. \\ \left.\left.\left.r^2\, cot^2\,\varphi\,\psi_1\delta\psi_1 + cot\,\varphi\,(\delta w_0 u_0 + w_0\delta u_0) + r(\delta w_0\psi_1 + w_0\delta\psi_1) + r\, cot\,\varphi\,(\delta u_0\psi_1 + u_0\delta\psi_1)\right)\right)\right) R^2\sin\varphi\, dr d\varphi d\theta\right) dt \end{gathered} \tag{31}$$

$$\delta U_c = \int_0^t \left(\iint_A I_1(-R\omega_E^2\sin^2\varphi\,\delta w_0 + R\omega_E^2\sin\varphi\, cos\,\varphi\,\delta u_0) R^2\sin\varphi\, d\varphi d\theta\right) dt \tag{32}$$

In the case of δU_ε, it can be reformulated by integrating into the r-direction which is the direction of the radius and thickness of the structure (similar to δU_k and δU_c). The average thickness of the Earth's crust is assumed as h. Also, the definition of stress and moment resultants N_{rr}, $N_{\varphi\varphi}$, $N_{\theta\theta}$, $N_{r\varphi}$, $M_{\varphi\varphi}$, $M_{\theta\theta}$, $M_{r\varphi}$, and mathematical resultants $P_{\varphi\varphi}$ and $P_{\theta\theta}$ are presented according to the below equations [19, 62]:

$$\delta U_{\varepsilon}=\int_0^t\Bigg(\int_{\theta_1}^{\theta_2}\int_{\varphi_1}^{\varphi_2}\Bigg(N_{rr}\psi_1\delta\psi_1+N_{r\varphi}\delta\psi_1+\frac{1}{R}\Big(N_{r\varphi}\frac{\partial\delta w_0}{\partial\varphi}-N_{r\varphi}\delta u_0-M_{r\varphi}\delta\psi_1\Big)+\frac{1}{R}\Big(\Big(N_{r\varphi}\frac{\partial u_0}{\partial\varphi}\delta\psi_1+N_{r\varphi}\psi_1\frac{\partial\delta u_0}{\partial\varphi}\Big)+\Big(M_{r\varphi}\frac{\partial\psi_1}{\partial\varphi}\delta\psi_1+M_{r\varphi}\psi_1\frac{\partial\delta\psi_1}{\partial\varphi}\Big)+\big(N_{r\varphi}w_0\delta\psi_1+N_{r\varphi}\psi_1\delta w_0\big)\Big)+\frac{1}{R}\Big(N_{\varphi\varphi}\frac{\partial\delta u_0}{\partial\varphi}+M_{\varphi\varphi}\frac{\partial\delta\psi_1}{\partial\varphi}+N_{\varphi\varphi}\delta w_0+\frac{1}{R}\Big(N_{\varphi\varphi}\Big(\frac{\partial w_0}{\partial\varphi}\Big)\Big(\frac{\partial\delta w_0}{\partial\varphi}\Big)+N_{\varphi\varphi}u_0\delta u_0+P_{\varphi\varphi}\psi_1\delta\psi_1-N_{\varphi\varphi}\Big(\frac{\partial w_0}{\partial\varphi}\Big)\delta u_0-N_{\varphi\varphi}u_0\Big(\frac{\partial\delta w_0}{\partial\varphi}\Big)-M_{\varphi\varphi}\Big(\frac{\partial w_0}{\partial\varphi}\Big)\delta\psi_1+M_{\varphi\varphi}\psi_1\Big(\frac{\partial\delta w_0}{\partial\varphi}\Big)+M_{\varphi\varphi}\psi_1\delta u_0+M_{\varphi\varphi}u_0\delta\psi_1+N_{\varphi\varphi}\Big(\frac{\partial u_0}{\partial\varphi}\Big)\Big(\frac{\partial\delta u_0}{\partial\varphi}\Big)+P_{\varphi\varphi}\Big(\frac{\partial\psi_1}{\partial\varphi}\Big)\Big(\frac{\partial\delta\psi_1}{\partial\varphi}\Big)+N_{\varphi\varphi}w_0\delta w_0+M_{\varphi\varphi}\Big(\frac{\partial\psi_1}{\partial\varphi}\Big)\Big(\frac{\partial\delta u_0}{\partial\varphi}\Big)+M_{\varphi\varphi}\Big(\frac{\partial u_0}{\partial\varphi}\Big)\Big(\frac{\partial\delta\psi_1}{\partial\varphi}\Big)+N_{\varphi\varphi}\Big(\frac{\partial u_0}{\partial\varphi}\Big)\delta w_0+N_{\varphi\varphi}w_0\Big(\frac{\partial\delta u_0}{\partial\varphi}\Big)+M_{\varphi\varphi}\Big(\frac{\partial\psi_1}{\partial\varphi}\Big)\delta w_0+M_{\varphi\varphi}w_0\Big(\frac{\partial\delta\psi_1}{\partial\varphi}\Big)\Big)\Big)+\frac{1}{R}\Big(\big(N_{\theta\theta}\delta w_0+(N_{\theta\theta}\delta u_0+M_{\theta\theta}\delta\psi_1)\cot\varphi\big)+\frac{1}{R}\big(N_{\theta\theta}w_0\delta w_0+N_{\theta\theta}u_0\cot^2\varphi\,\delta u_0+P_{\theta\theta}\psi_1\cot^2\varphi\,\delta\psi_1+(N_{\theta\theta}u_0\delta w_0+N_{\theta\theta}w_0\delta u_0)\cot\varphi+M_{\theta\theta}\psi_1\delta w_0+M_{\theta\theta}w_0\delta\psi_1+(M_{\theta\theta}\psi_1\delta u_0+M_{\theta\theta}u_0\delta\psi_1)\cot\varphi\big)\Big)R^2\sin\varphi\,d\varphi d\theta\Bigg)dt \tag{33}$$

$$\begin{cases}(N_{rr},N_{r\varphi},N_{\varphi\varphi},N_{\theta\theta})=\int_{-\frac{h}{2}}^{\frac{h}{2}}(\sigma_{rr},\sigma_{r\varphi},\sigma_{\varphi\varphi},\sigma_{\theta\theta})dr\\(M_{rr},M_{r\varphi},M_{\varphi\varphi},M_{\theta\theta})=\int_{-\frac{h}{2}}^{\frac{h}{2}}(\sigma_{rr},\sigma_{r\varphi},\sigma_{\varphi\varphi},\sigma_{\theta\theta})rdr\\(P_{\varphi\varphi},P_{\theta\theta})=\int_{-\frac{h}{2}}^{\frac{h}{2}}(\sigma_{\varphi\varphi},\sigma_{\theta\theta})r^2dr\end{cases} \tag{34}$$

Finally, by substituting the obtained results into Equation (24), the dynamic governing equations will be obtained. In Hooke's law, $\vec{\sigma}_{ij}=C:\vec{\varepsilon}_{ij}$ the matrix C is the stiffness matrix of the material. The material properties in the Earth's crust are assumed uniformly in all orientations (isotropic material). The dimension of the matrix C is 4×4 in which E and ν are Young's modulus and Poisson's ratio of the Earth's crust respectively [19, 62]:

$$\begin{bmatrix}\sigma_{rr}\\\sigma_{\varphi\varphi}\\\sigma_{\theta\theta}\\\sigma_{r\varphi}\end{bmatrix}=\frac{E}{(1-\nu^2)}\begin{bmatrix}1&\nu&\nu&0\\\nu&1&\nu&0\\\nu&\nu&1&0\\0&0&0&(1-\nu)\end{bmatrix}\begin{bmatrix}\varepsilon_{rr}\\\varepsilon_{\varphi\varphi}\\\varepsilon_{\theta\theta}\\\varepsilon_{r\varphi}\end{bmatrix} \tag{35}$$

Material characteristics for the Earth's layers can be studied and considered due to previous research [63-65]. Finally, by adding the equivalent values of δu_0, δw_0, and $\delta\psi_1$ (in Equation (24)), dynamic governing equations of the planet Earth will be extracted. Obtained dynamic equations are completely nonlinear in both directions r and φ. The mathematical modeling simulates the deformation and tectonic motions of the Earth's layers due to its internal pressures in the longitudinal (U_{φ}) and radial (U_r) orientations:

$$\delta u_0:-\Big(\cot\varphi\,N_{r\varphi}\psi_1+\Big(\frac{\partial N_{r\varphi}}{\partial\varphi}\Big)\psi_1+N_{r\varphi}\Big(\frac{\partial\psi_1}{\partial\varphi}\Big)\Big)+\frac{1}{R}\left(N_{\varphi\varphi}u_0+M_{\varphi\varphi}\psi_1\right)-\frac{1}{R}\Big(N_{\varphi\varphi}\Big(\frac{\partial w_0}{\partial\varphi}\Big)-\cot\varphi\,N_{\varphi\varphi}\Big(\frac{\partial u_0}{\partial\varphi}\Big)-\Big(\frac{\partial N_{\varphi\varphi}}{\partial\varphi}\Big)\Big(\frac{\partial u_0}{\partial\varphi}\Big)-N_{\varphi\varphi}\Big(\frac{\partial^2u_0}{\partial^2\varphi}\Big)\Big)-\frac{1}{R}\Big(\cot\varphi\,M_{\varphi\varphi}\Big(\frac{\partial\psi_1}{\partial\varphi}\Big)+\Big(\frac{\partial M_{\varphi\varphi}}{\partial\varphi}\Big)\Big(\frac{\partial\psi_1}{\partial\varphi}\Big)+M_{\varphi\varphi}\Big(\frac{\partial^2\psi_1}{\partial^2\varphi}\Big)\Big)-\frac{1}{R}\Big(\cot\varphi\,N_{\varphi\varphi}w_0+\Big(\frac{\partial N_{\varphi\varphi}}{\partial\varphi}\Big)w_0+N_{\varphi\varphi}\Big(\frac{\partial w_0}{\partial\varphi}\Big)\Big)+\frac{1}{R}\cot^2\varphi\,(N_{\theta\theta}u_0+M_{\theta\theta}\psi_1)+\frac{1}{R}(\cot\varphi\,N_{\theta\theta}w_0-RN_{r\varphi})-\Big(\Big(\frac{\partial N_{\varphi\varphi}}{\partial\varphi}\Big)+\cot\varphi\,(N_{\varphi\varphi}-N_{\theta\theta})\Big)-Rq_{\varphi}+I_1R^2\omega_E^2\sin\varphi\cos\varphi+R\Big(I_1\frac{\partial^2u_0}{\partial t^2}+I_2\frac{\partial^2\psi_1}{\partial t^2}\Big)=0 \tag{36}$$

$$\delta w_0:R\sin\varphi\,N_{r\varphi}\psi_1-\frac{\partial}{\partial\varphi}\Big(\sin\varphi\,N_{\varphi\varphi}\Big(\frac{\partial w_0}{\partial\varphi}\Big)\Big)+\frac{\partial}{\partial\varphi}(\sin\varphi\,N_{\varphi\varphi}u_0)+\frac{\partial}{\partial\varphi}(\sin\varphi\,M_{\varphi\varphi}\psi_1)+\sin\varphi\,N_{\varphi\varphi}w_0+\sin\varphi\,N_{\theta\theta}w_0+\cot\varphi\sin\varphi\,N_{\theta\theta}u_0+\cot\varphi\sin\varphi\,M_{\theta\theta}\psi_1-\frac{\partial}{\partial\varphi}(R\sin\varphi\,N_{r\varphi})+R\sin\varphi\,N_{\varphi\varphi}+R\sin\varphi\,N_{\theta\theta}-q_rR^2\sin\varphi+\sin\varphi\,N_{\varphi\varphi}\Big(\frac{\partial u_0}{\partial\varphi}\Big)+\sin\varphi\,M_{\varphi\varphi}\Big(\frac{\partial\psi_1}{\partial\varphi}\Big)-I_1R^3\omega_E^2\sin^3\varphi+R^2\sin\varphi\Big(I_1\frac{\partial^2w_0}{\partial t^2}\Big)=0 \tag{37}$$

$$\delta\psi_1:R\sin\varphi\,N_{r\varphi}w_0+R\sin\varphi\,N_{r\varphi}\Big(\frac{\partial u_0}{\partial\varphi}\Big)+R\sin\varphi\,M_{r\varphi}\Big(\frac{\partial\psi_1}{\partial\varphi}\Big)-\frac{\partial}{\partial\varphi}(R\sin\varphi\,M_{r\varphi}\psi_1)+\sin\varphi\,P_{\varphi\varphi}\psi_1+\sin\varphi\,M_{\varphi\varphi}u_0-\sin\varphi\,M_{\varphi\varphi}\Big(\frac{\partial w_0}{\partial\varphi}\Big)-\frac{\partial}{\partial\varphi}\Big(\sin\varphi\,P_{\varphi\varphi}\Big(\frac{\partial\psi_1}{\partial\varphi}\Big)\Big)-\frac{\partial}{\partial\varphi}\Big(\sin\varphi\,M_{\varphi\varphi}\Big(\frac{\partial u_0}{\partial\varphi}\Big)\Big)-\frac{\partial}{\partial\varphi}(\sin\varphi\,M_{\varphi\varphi}w_0)+\cot^2\varphi\sin\varphi\,P_{\theta\theta}\psi_1+\cot^2\varphi\sin\varphi\,M_{\theta\theta}u_0+\cot\varphi\sin\varphi\,M_{\theta\theta}w_0-R\sin\varphi\,M_{r\varphi}+R^2\sin\varphi\,N_{r\varphi}-\frac{\partial}{\partial\varphi}(R\sin\varphi\,M_{\varphi\varphi})+R\sin\varphi\cot\varphi\,M_{\theta\theta}+q_{\varphi}(\tfrac{h}{2})R^2\sin\varphi+R^2\sin\varphi\Big(I_2\frac{\partial^2u_0}{\partial t^2}+I_3\frac{\partial^2\psi_1}{\partial t^2}\Big)=0 \tag{38}$$

5. Quasi Three-dimensional Theories

5.1. Simplified quasi-three-dimensional theory (SQT)

It has already been stated that if the ratio of the radius of the Earth to its thickness is less than a value (R/h < 10), theories that do not consider strain in the direction of thickness can no longer be used. The use of exact three-dimensional theories also has its own difficulties. Thus, quasi-three-dimensional theories can be used for this purpose. In this research, a simplified quasi-three-dimensional theory presented by the authors of the research has been used to mechanically model a spherical structure that is actually a shell structure. In this theory, (SQT) [66] only by adding an unknown function to the displacement field, three-dimensional results can be obtained. The displacement field in this theory will be as the following equations (for a complete spherical structure that changes are only in the direction of φ):

$$\begin{cases}U_{\varphi}(r,\varphi,t)=u_0(\varphi,t)+f(r).\,\psi_1(\varphi,t)\\U_{\theta}(r,\varphi,t)=0\\U_r(r,\varphi,t)=w_0(\varphi,t)+g(r).\,w_1(\varphi,t)\end{cases} \tag{39}$$

Now, by considering the introduced strain field (Equation (39)) in the strain energy changes (Equation (25)), the strain field can be obtained as the preceding described process. Finally, quasi-three-dimensional dynamic equations based on SQT with the resulting components of stress and moment resultants can be obtained based on $\delta u_0,\delta\psi_1,\delta w_0$ and δw_1 variations as the following equations (the nonlinear terms in strain field are neglected):

$$\delta U_k = -\int_0^t \left(\iiint_V \rho \left(\left(\frac{\partial U_\varphi}{\partial t}\frac{\partial \delta U_\varphi}{\partial t}\right) + \left(\frac{\partial U_r}{\partial t}\frac{\partial \delta U_r}{\partial t}\right)\right) dV \right) dt = -\int_0^t \left(\iiint_V \rho \left(\left(\frac{\partial u_0}{\partial t} + f(r)\frac{\partial \psi_1}{\partial t}\right)\left(\frac{\partial \delta u_0}{\partial t} + f(r)\frac{\partial \delta \psi_1}{\partial t}\right) + \left(\frac{\partial w_0}{\partial t} + g(r)\frac{\partial w_1}{\partial t}\right)\left(\frac{\partial \delta w_0}{\partial t} + g(r)\frac{\partial \delta w_1}{\partial t}\right)\right) dV \right) dt = -\int_0^t \left(\int_{\varphi_1}^{\varphi_2}\int_{\theta_1}^{\theta_2} \left(\left(I_1\left(\frac{\partial u_0}{\partial t}\frac{\partial \delta u_0}{\partial t}\right) + I_2\left(\frac{\partial u_0}{\partial t}\frac{\partial \delta \psi_1}{\partial t} + \frac{\partial \psi_1}{\partial t}\frac{\partial \delta u_0}{\partial t}\right) + I_3\left(\frac{\partial \psi_1}{\partial t}\frac{\partial \delta \psi_1}{\partial t}\right) + I_1\left(\frac{\partial w_0}{\partial t}\frac{\partial \delta w_0}{\partial t}\right) + I_4\left(\frac{\partial w_0}{\partial t}\frac{\partial \delta w_1}{\partial t} + \frac{\partial w_1}{\partial t}\frac{\partial \delta w_0}{\partial t}\right) + I_5\left(\frac{\partial w_1}{\partial t}\frac{\partial \delta w_1}{\partial t}\right)\right)\right) R^2 \sin\varphi \, d\varphi d\theta \right) dt \quad (I_1, I_2, I_3) = \int_{-\frac{h}{2}}^{\frac{h}{2}} \rho \left(1, f(r), (f(r))^2\right) dr \, ; (I_4, I_5) = \int_{-\frac{h}{2}}^{\frac{h}{2}} \rho \left(g(r), (g(r))^2\right) dr \tag{40}$$

$$\delta U_c = \int_0^t \left(\iint_A \left(-R\omega_E^2 \sin^2\varphi \left(\delta w_0 + g(r)\delta w_1\right) + R\omega_E^2 \sin\varphi\cos\varphi \left(\delta u_0 + f(r)\delta\psi_1\right)\right) R^2 \sin\varphi \, d\varphi d\theta \right) dt \tag{41}$$

The governing equations based on the SQT analysis:

$$\delta u_0 : N_{r\varphi} + \left(\frac{\partial N_{\varphi\varphi}}{\partial \varphi}\right) + cot\,\varphi \left(N_{\varphi\varphi} - N_{\theta\theta}\right) + Rq_\varphi - I_1 R^2 \omega_E^2 \sin\varphi\cos\varphi + R\left(I_1\frac{\partial^2 u_0}{\partial t^2} + I_2\frac{\partial^2 \psi_1}{\partial t^2}\right) = 0 \tag{42}$$

$$\delta \psi_1 : RK_{r\varphi} - P_{r\varphi} - \left(\frac{\partial P_{\varphi\varphi}}{\partial \varphi}\right) + cot\,\varphi \left(P_{\theta\theta} - P_{\varphi\varphi}\right) + Rq_\varphi \left(f(r)|_{r=-\frac{h}{2}}\right) - I_2 R^2 \omega_E^2 \sin\varphi\cos\varphi + R\left(I_2\frac{\partial^2 u_0}{\partial t^2} + I_3\frac{\partial^2 \psi_1}{\partial t^2}\right) = 0 \tag{43}$$

$$\delta w_0 : \left(\frac{\partial N_{r\varphi}}{\partial \varphi}\right) + \cot\varphi \, N_{r\varphi} - \left(N_{\varphi\varphi} + N_{\theta\theta}\right) + Rq_r + I_1 R^2 \omega_E^2 \sin^2\varphi + R\left(I_1\frac{\partial^2 w_0}{\partial t^2} + I_4\frac{\partial^2 w_1}{\partial t^2}\right) = 0 \tag{44}$$

$$\delta w_1 : \left(\frac{\partial H_{r\varphi}}{\partial \varphi}\right) + \cot\varphi \, H_{r\varphi} - RK_{rr} - \left(H_{\varphi\varphi} + H_{\theta\theta}\right) + Rq_r \left(g(r)|_{r=-\frac{h}{2}}\right) + I_4 R^2 \omega_E^2 \sin^2\varphi + R\left(I_4\frac{\partial^2 w_0}{\partial t^2} + I_5\frac{\partial^2 w_1}{\partial t^2}\right) = 0 \tag{45}$$

$$\begin{cases} \left(N_{r\varphi}, N_{\varphi\varphi}, N_{\theta\theta}\right) = \int_{-\frac{h}{2}}^{\frac{h}{2}} \left(\sigma_{r\varphi}, \sigma_{\varphi\varphi}, \sigma_{\theta\theta}\right) dr \\ \left(H_{r\varphi}, H_{\varphi\varphi}, H_{\theta\theta}\right) = \int_{-\frac{h}{2}}^{\frac{h}{2}} \left(\sigma_{r\varphi}, \sigma_{\varphi\varphi}, \sigma_{\theta\theta}\right) g(r) dr \\ \left(P_{r\varphi}, P_{\varphi\varphi}, P_{\theta\theta}\right) = \int_{-\frac{h}{2}}^{\frac{h}{2}} \left(\sigma_{r\varphi}, \sigma_{\varphi\varphi}, \sigma_{\theta\theta}\right) f(r) dr \end{cases} \quad \begin{cases} K_{rr} = \int_{-\frac{h}{2}}^{\frac{h}{2}} \sigma_{rr} \left(\frac{df(r)}{dr}\right) dr \\ K_{r\varphi} = \int_{-\frac{h}{2}}^{\frac{h}{2}} \sigma_{r\varphi} \left(\frac{dg(r)}{dr}\right) dr \end{cases} \tag{46}$$

5.2. Polynomial quasi-three-dimensional theory (PQT)

It is observed that the proposed quasi-three-dimensional theory (SQT) [67] considers the strain variations through the thickness ($\varepsilon_{rr} \neq 0$). To aim obtaining more accurate results, another quasi-three-dimensional theory based on polynomial functions is presented in this research. The mathematical formulation of the strain field can be proposed as a set of a polynomial system below:

$$\begin{cases} U_\varphi(r,\varphi,t) = \sum_{i=0}^{N} r^i u_i(\varphi,t) \\ U_\theta(r,\varphi,t) = \sum_{i=0}^{N} r^i v_i(\varphi,t) \\ U_r(r,\varphi,t) = \sum_{i=0}^{N} r^i w_i(\varphi,t) \end{cases} \tag{47}$$

The unknown functions $u_i(\varphi,t)$, $v_i(\varphi,t)$ and $w_i(\varphi,t)$, $(i = 0\,..\,N)$ will be calculated after solving the governing equations. Whatever N is greater, the obtained results will be more than the same as the exact three-dimensional analysis. However, the greater amount of N causes more unknown functions and in consequence the number of governing equations. To avoid massive calculations and also obtain the appropriate results, the parameter N has been chosen as $N = 3$ for symmetric assumptions as in SQT analysis. So, the number of 8 unknowns and resulting governing equations will be extracted. The strain field in Equation (47) will be refined as follows:

$$\begin{cases} U_\varphi(r,\varphi,t) = \sum_{i=0}^{3} r^i u_i(\varphi,t) \\ U_\theta(r,\varphi,t) = 0 \\ U_r(r,\varphi,t) = \sum_{i=0}^{3} r^i w_i(\varphi,t) \end{cases} \tag{48}$$

After a complete similar explained process in Sections 4 and 5.1, the dynamic governing equations and the resultant components are derived as below:

$$\delta u_0 : N_{r\varphi} + \left(\frac{\partial N_{\varphi\varphi}}{\partial \varphi}\right) + \cot\varphi \left(N_{\varphi\varphi} - N_{\theta\theta}\right) + Rq_\varphi - I_1 R^2 \omega_E^2 \sin\varphi\cos\varphi + R\left(I_1\frac{\partial^2 u_0}{\partial t^2} + I_2\frac{\partial^2 u_1}{\partial t^2} + I_3\frac{\partial^2 u_2}{\partial t^2} + I_4\frac{\partial^2 u_3}{\partial t^2}\right) = 0 \tag{49}$$

$$\delta u_1 : -RN_{r\varphi} + \left(\frac{\partial M_{\varphi\varphi}}{\partial \varphi}\right) + M_{r\varphi} + \cot\varphi \left(M_{\varphi\varphi} - M_{\theta\theta}\right) + Rq_{r\varphi}\left(-\tfrac{h}{2}\right) - I_2 R^2 \omega_E^2 \sin\varphi\cos\varphi + R\left(I_2\frac{\partial^2 u_0}{\partial t^2} + I_3\frac{\partial^2 u_1}{\partial t^2} + I_4\frac{\partial^2 u_2}{\partial t^2} + I_5\frac{\partial^2 u_3}{\partial t^2}\right) = 0 \tag{50}$$

$$\delta u_2 : -2RM_{r\varphi} + \left(\frac{\partial P_{\varphi\varphi}}{\partial \varphi}\right) + P_{r\varphi} + \cot\varphi \left(P_{\varphi\varphi} - P_{\theta\theta}\right) + Rq_\varphi\left(-\tfrac{h}{2}\right)^2 - I_3 R^2 \omega_E^2 \sin\varphi\cos\varphi + R\left(I_3\frac{\partial^2 u_0}{\partial t^2} + I_4\frac{\partial^2 u_1}{\partial t^2} + I_5\frac{\partial^2 u_2}{\partial t^2} + I_6\frac{\partial^2 u_3}{\partial t^2}\right) = 0 \tag{51}$$

$$\delta u_3 : -3RP_{r\varphi} + \left(\frac{\partial H_{\varphi\varphi}}{\partial \varphi}\right) + H_{r\varphi} + \cot\varphi \left(H_{\varphi\varphi} - H_{\theta\theta}\right) + Rq_\varphi\left(-\tfrac{h}{2}\right)^3 - I_4 R^2 \omega_E^2 \sin\varphi\cos\varphi + R\left(I_4\frac{\partial^2 u_0}{\partial t^2} + I_5\frac{\partial^2 u_1}{\partial t^2} + I_6\frac{\partial^2 u_2}{\partial t^2} + I_7\frac{\partial^2 u_3}{\partial t^2}\right) = 0 \tag{52}$$

$$\delta w_0 : \left(\frac{\partial N_{r\varphi}}{\partial \varphi}\right) + \cot\varphi \, N_{r\varphi} - \left(N_{\varphi\varphi} + N_{\theta\theta}\right) + Rq_r + I_1 R^2 \omega_E^2 \sin^2\varphi + R\left(I_1\frac{\partial^2 w_0}{\partial t^2} + I_2\frac{\partial^2 w_1}{\partial t^2} + I_3\frac{\partial^2 w_2}{\partial t^2} + I_4\frac{\partial^2 w_3}{\partial t^2}\right) = 0 \tag{53}$$

$$\delta w_1: -RN_{rr} + \left(\frac{\partial M_{r\varphi}}{\partial \varphi}\right) + \cot\varphi\, M_{r\varphi} - (M_{\varphi\varphi} + M_{\theta\theta}) + Rq_r(-\tfrac{h}{2}) + I_2R^2\omega_E^2\sin^2\varphi + R\left(I_2\frac{\partial^2 w_0}{\partial t^2} + I_3\frac{\partial^2 w_1}{\partial t^2} + I_4\frac{\partial^2 w_2}{\partial t^2} + I_5\frac{\partial^2 w_3}{\partial t^2}\right) = 0 \tag{54}$$

$$\delta w_2: -2RM_{rr} + \left(\frac{\partial P_{r\varphi}}{\partial \varphi}\right) + \cot\varphi\, P_{r\varphi} - (P_{\varphi\varphi} + P_{\theta\theta}) + Rq_r(-\tfrac{h}{2})^2 + I_3R^2\omega_E^2\sin^2\varphi + R\left(I_3\frac{\partial^2 w_0}{\partial t^2} + I_4\frac{\partial^2 w_1}{\partial t^2} + I_5\frac{\partial^2 w_2}{\partial t^2} + I_6\frac{\partial^2 w_3}{\partial t^2}\right) = 0 \tag{55}$$

$$\delta w_3: -3RP_{rr} + \left(\frac{\partial H_{r\varphi}}{\partial \varphi}\right) + \cot\varphi\, H_{r\varphi} - (H_{\varphi\varphi} + H_{\theta\theta}) + Rq_r(-\tfrac{h}{2})^3 + I_4R^2\omega_E^2\sin^2\varphi + R\left(I_4\frac{\partial^2 w_0}{\partial t^2} + I_5\frac{\partial^2 w_1}{\partial t^2} + I_6\frac{\partial^2 w_2}{\partial t^2} + I_7\frac{\partial^2 w_3}{\partial t^2}\right) = 0 \tag{56}$$

$$\begin{cases} (N_{rr}, N_{r\varphi}, N_{\varphi\varphi}, N_{\theta\theta}) = \int_{-\frac{h}{2}}^{\frac{h}{2}} (\sigma_{rr}, \sigma_{r\varphi}, \sigma_{\varphi\varphi}, \sigma_{\theta\theta}) dr \\ (M_{rr}, M_{r\varphi}, M_{\varphi\varphi}, M_{\theta\theta}) = \int_{-\frac{h}{2}}^{\frac{h}{2}} (\sigma_{rr}, \sigma_{r\varphi}, \sigma_{\varphi\varphi}, \sigma_{\theta\theta}) r dr \\ (P_{rr}, P_{r\varphi}, P_{\varphi\varphi}, P_{\theta\theta}) = \int_{-\frac{h}{2}}^{\frac{h}{2}} (\sigma_{rr}, \sigma_{r\varphi}, \sigma_{\varphi\varphi}, \sigma_{\theta\theta}) r^2 dr \\ (H_{rr}, H_{r\varphi}, H_{\varphi\varphi}, H_{\theta\theta}) = \int_{-\frac{h}{2}}^{\frac{h}{2}} (\sigma_{rr}, \sigma_{r\varphi}, \sigma_{\varphi\varphi}, \sigma_{\theta\theta}) r^3 dr \end{cases} \tag{57}$$

$$(I_1, I_2, I_3, I_4, I_5, I_6, I_7) = \int_{-\frac{h}{2}}^{\frac{h}{2}} \rho(1, r, r^2, r^3, r^4, r^5, r^6) dr \tag{58}$$

There are so many available solution methods to solve the derived governing equations. Due to simple formulations and also obtaining appropriate and accurate results, SAPM is used by the authors in this research. Formulations and discussions about this method have been explained in detail in previous papers [12-14]. Consequently, explanations for solving the process of governing equations have been omitted because of avoiding duplications, and instead, it is tried to focus on more important issues in the next part (numerical analysis and discussion).

6. Numerical Results

Given that the pressure in the inner layers of the Earth increases with increasing depth in the layers from the Earth's surface, the effects of this increase in depth on the deformation created at different depths can be calculated. First, the common boundary between the inner core and the outer core is calculated, and the radial deformations w as well as the deformations created in the latitude (U_φ) direction will be calculated. The depth from the ground to the inner core boundary is about 5155 km. Therefore, the desired thickness *h* to analyze the spherical structure of the Earth will be assumed to be equal to the same depth mentioned. In advance, as can be expected, the changes in the radial direction (*r*) should be significant. In other words, due to the fact that the thickness of the spherical structure is considered to be very thick, it should be the maximum amount of deformation inside the Earth and the common boundary of the outer and inner core and gradually reduce the intensity of deformation by distance from the depth. In Figures 5a and b, the radial deformations of w and U_φ are observed with respect to the changes of the variables in r and φ directions. In the case of Figure 5a, it is observed that the deformation of the inner layers of the Earth in the direction of φ for different values of angles follows an almost similar trend. This uniform behavior will be much more dramatic in the depths of the Earth, and with increasing depth to values close to the Earth's surface, fluctuations in the amount of w regarding the φ angle will be observed. It can be seen that from angles close to zero and 180°, which actually represent the location of the Earth's poles, towards the equator, the amount of radial deformation of the Earth's layers fluctuates, or in other words, at two specific angles in the northern and southern hemispheres, the value of w is highest. By moving away from these two regions, the value of w will reach its lowest value at the equator. As mentioned earlier, changes in w along the radius (*r*) experience large fluctuations, and if a non-three-dimensional analysis was used, significant errors would be made that would make it impossible to use the results. Changes in U_φ deformation do not follow a regular pattern. The remarkable thing is the maximum and minimum amount of U_φ that is created on the surface of the Earth. In the northern and southern hemispheres, these maximum values are equal and symmetrical to each other. As can be seen in the equator, the U_φ deformations have the lowest possible value (in terms of absolute magnitude). Of course, it can be concluded that there are many areas in which the value of U_φ equals zero.

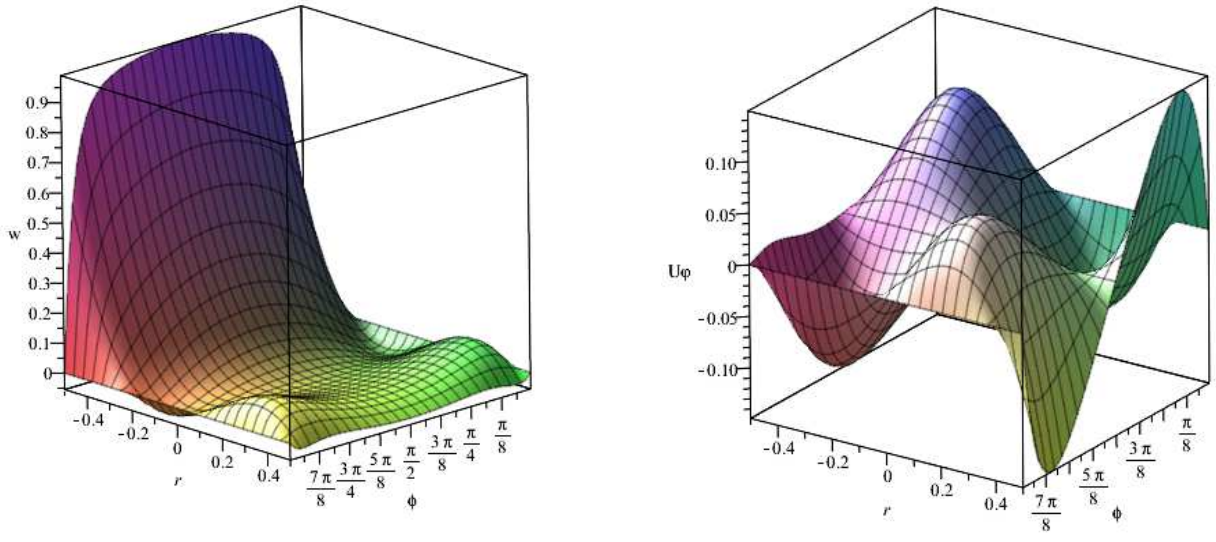

(a) (b)

Fig. 5. Movement of the Earth's layers under pressure applied on common boundary between inner and outer core for (a) radial w (b) shear U_φ displacement.

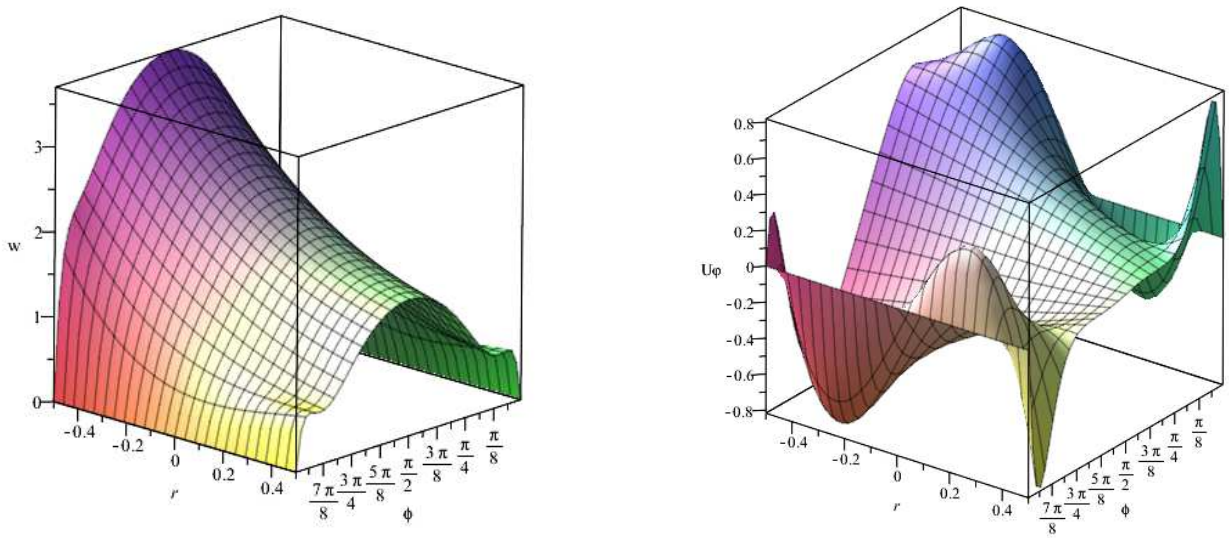

(a) (b)

Fig. 6. Movement of the Earth's layers under pressure applied on common boundary between the outer core and lower mantle for (a) radial w (b) shear U_φ displacement.

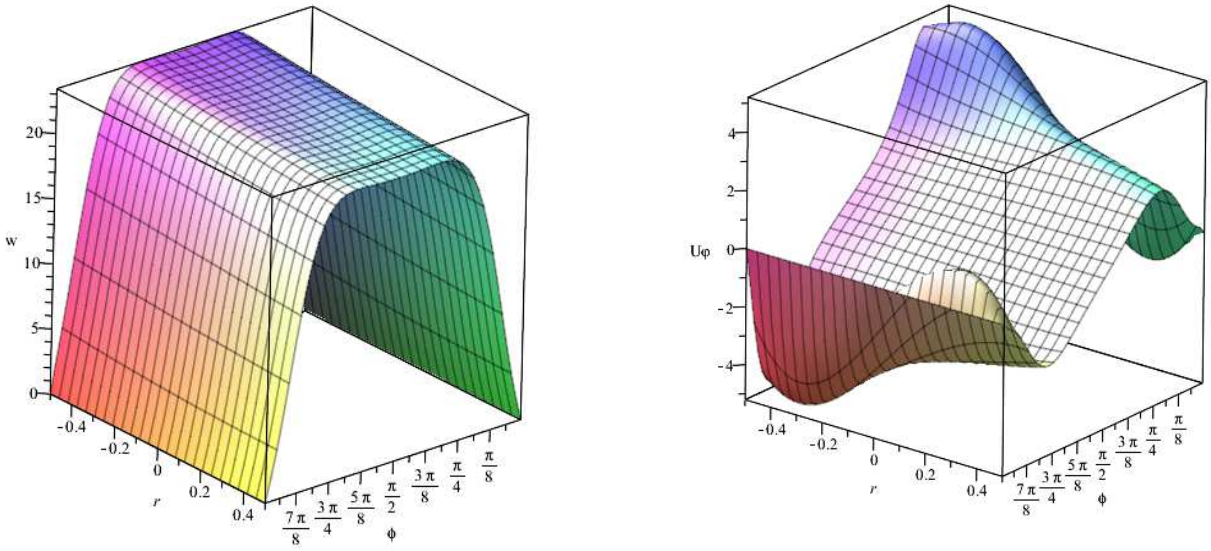

(a) (b)

Fig. 7. Movement of the Earth's layers under pressure applied on common boundary between the lower mantle and upper mantle for (a) radial w (b) shear U_φ displacement.

In Figures 5a and 5b, the assumed and analyzed layer considered the common boundary between the inner and outer core. Now, the boundary between the outer core and the lower mantle is assumed. Obviously, the pressure on this boundary will be less than the pressure on the surface of the inner core. Figures 6a and 6b (similar to the conditions in Figures 5a and 5b) show the effect of pressures on the boundary between the outer core and the lower mantle on the deformation of the layers above the lower mantle to the ground. Here the changes w will be more uniform than before (Figure 5a). But since the pressure on the layer above the inner core is assumed, the slope of the changes along the radius axis (r) will be less than in Figure 5a. However, there are still significant changes in the radius direction. In other words, at the interface between the outer core and the lower mantle, the maximum value of w is approximately 3.75 km. But this value is about 1.5 km (2.5 times less) on the outer surface of the Earth's crust. The changes mentioned in Figure 5a show approximately a 9-fold reduction from the interface boundary between the inner and outer core to the outer surface of the Earth's crust. Unlike Figure 5a, there is no fluctuation of the results in r and φ directions, and there will be a maximum value of w in the equator. The results for U_φ values can be compared with the results obtained in Figure 5b, and by evaluating the results, it can be seen that the trend of changes is similar. But the important difference is that most of the changes in the amount of U_φ are in the inner layer and not in the surface layer of the Earth. Therefore, the closer we get to the upper layers and closer to the adjacent surface to the atmosphere, the greater the amount of displacement and deformation. The U_φ displacement diagram provides researchers with very important information about the amount of latitude displacement of the Earth's inner plates. The obtained results can be used and studied in predicting the movements of the inner layers of the Earth, especially before the occurrence of earthquakes. Comparing the results obtained in Figures 6a and b, it can be seen that there is more relative complexity in the analysis of U_φ displacements than in w. One of the prominent and important features of this research is the mathematical modeling of the movement of the Earth's layers at different depths in both r and φ directions. Of course, it should be noted that all these models are non-linear and completely dynamic in order to be most compatible with reality.

In the last step, the results of the deformation of w and U_φ for the pressure created at the interface between the lower mantle and the upper mantle will be examined. Figures 7a and 7b are drawn for this purpose. As can be seen, because the simulated

structure of the Earth is no longer in the range of a thick structure, the changes w along the r (radius) are negligible. Also, in a wide range of φ angles, the value of w will be constant and its value will be maximum. However, the mentioned result (approximate constant of the results w in the radial direction r) is not correct for the U_φ values and it is observed that in the areas close to the poles the changes of the U_φ in the radial direction are significant. But moving away from the Arctic and Antarctic regions, the U_φ changes with respect to the Earth's radius axis are almost uniform. Also, in the tropics, the U_φ value is almost zero. According to Figures 5 to 7, a good understanding of the mobility of the Earth's inner layers in different directions can be obtained. If a trend as animation is obtained from Figures 5 to 7, the rate of change can be seen in the form of dynamic 3D charts. A general result that can be obtained relatively from three shapes 1 to 3 is the small amount of movement of the Earth's layers in the latitude direction near the equator. Also, in contrast to the U_φ transverse displacement, the value of the radial displacement w in the tropics is significant and will have a maximum value. It can be modeled that the radial displacements w cause the vertical earthquakes and the U_φ transverse displacements will cause the transverse earthquakes. This research, as mentioned before, it has been tried to be as similar as possible to the proposed model with the theoretical foundations of the problem. Of course, the discussion of details will be very complex, and not all the factors influencing the model can be considered because the factors will be very large. The presentation of a three-dimensional mathematical model in this research can largely simulate the effects of displacement of layers in the ground in general. In order to understand the superiority of the presented three-dimensional model in this study compared to other models, the results of a two-dimensional model are also presented. So far, however, not even a two-dimensional mathematical model has been proposed to simulate the movements of the Earth's inner layers.

As mentioned, the problem would be much simpler if only changes in the φ direction were considered, but the results would no longer be accurate enough. The inaccuracy of the results is very important when the structure under analysis is much thicker than other dimensions. Figures 8a and 8b show the changes in w and U_φ relative to the changes in φ. The considered layer in this analysis is the common boundary between the inner core and the outer core. There is a very clear difference between the results of two-dimensional analysis (Figures 8a and 8b) and three-dimensional analysis (Figures 5a and 5b). Therefore, in the mathematical analysis and simulation of the Earth's layers, in terms of studying the resulting deformations, three-dimensional equations must be used. Not using 3D equations will cause serious errors in the results. Consequently, the numerical results obtained from the two-dimensional analysis will be invalidated.

In this study, the pressure inside the Earth, which is a function of the depth basis (from the surface of the Earth) is not only considered in the direction of radius r, but also in the direction of φ, it is assumed that a shear pressure at the assumed surface is applied. Applying pressure in the direction of φ can affect the results. In practice, there are such pressures that not much information is available about the actual amount of these pressures. Therefore, in the present study, the q_φ value is considered as a percentage of the q_r pressure and the results will be obtained based on it. The primary criterion for comparing the results here is that the q_φ pressure is zero. Two values are assumed for q_φ and the results of the displacements w and U_φ are shown in Figures 9 and 10. The problem conditions for the two forms mentioned are as follows:

$$q_\varphi = 0.1 q_r$$
$$q_\varphi = 0.5 q_r \tag{59}$$

It can be seen from Figure 9a that the trend of changes w for the two modes 1 and 2 is very similar. But the maximum value for w_1 is greater than w_0. Of course, there is not much difference between the results (Fig. 9a). As the value of q_φ increases from $0.1q_r$ to $0.5q_r$, the difference between the results of w_2 and w_0 increases. The noteworthy point is the obvious difference in the trend of changes w_2 and w_0 with respect to the two axes r and φ. It can be seen that the changes in the φ direction will be sinusoidal. The remarkable thing about Figures 9a and 9b are that the location of the common denominator between diagrams w_1 and w_0 and diagrams w_2 and w_0 will be almost the same. The higher the q_φ value, the greater the change in radial displacement (w). But this increase is not commensurate with the increase in q_φ, and it seems that there is a decreasing trend between increasing q_φ and increasing w. The change in direction of the value of w_2 will occur approximately at the equator ($\varphi = \pi/2$) and the trend of change in the two hemispheres is almost the same regardless of the sign w.

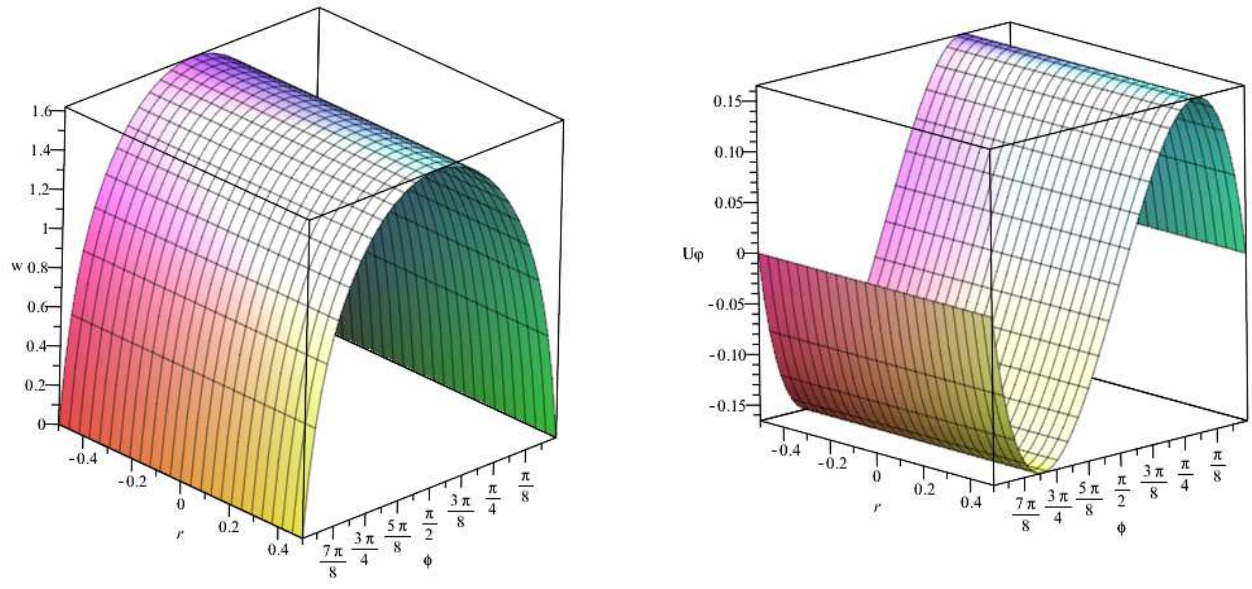

(a) (b)

Fig. 8. Two-dimensional analysis of Earth's layers under pressure applied on common boundary between inner and outer core for (a) radial w (b) shear U_φ displacements.

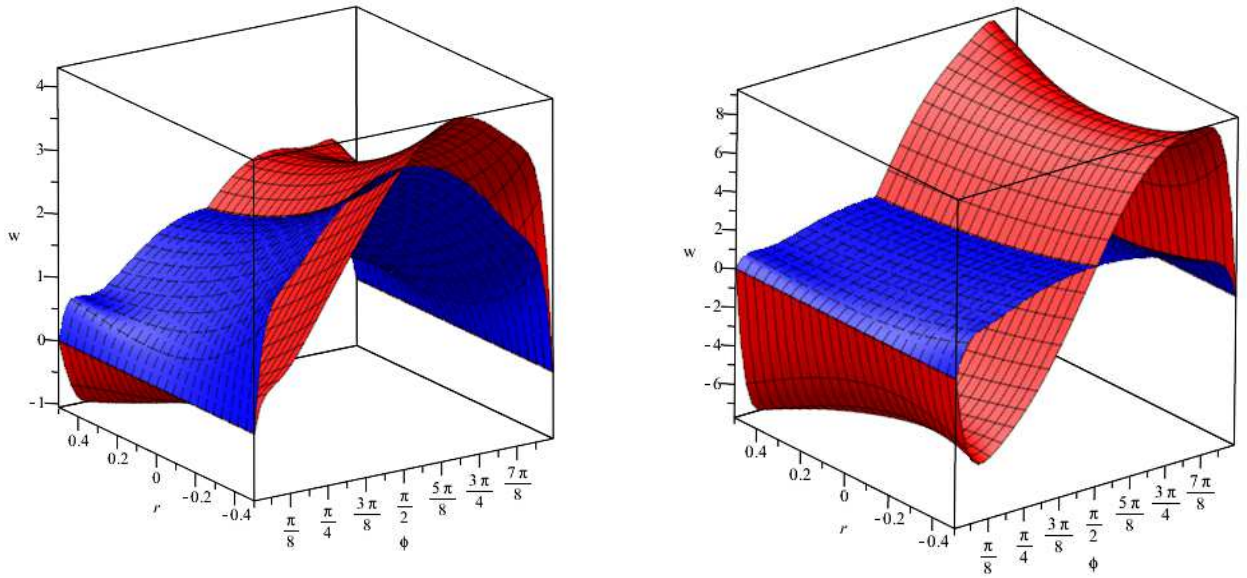

Fig. 9. Comparison between the radial layer's movement (w) for (a) $q_\varphi = 0.1q_r$ (b) $q_\varphi = 0.5q_r$.

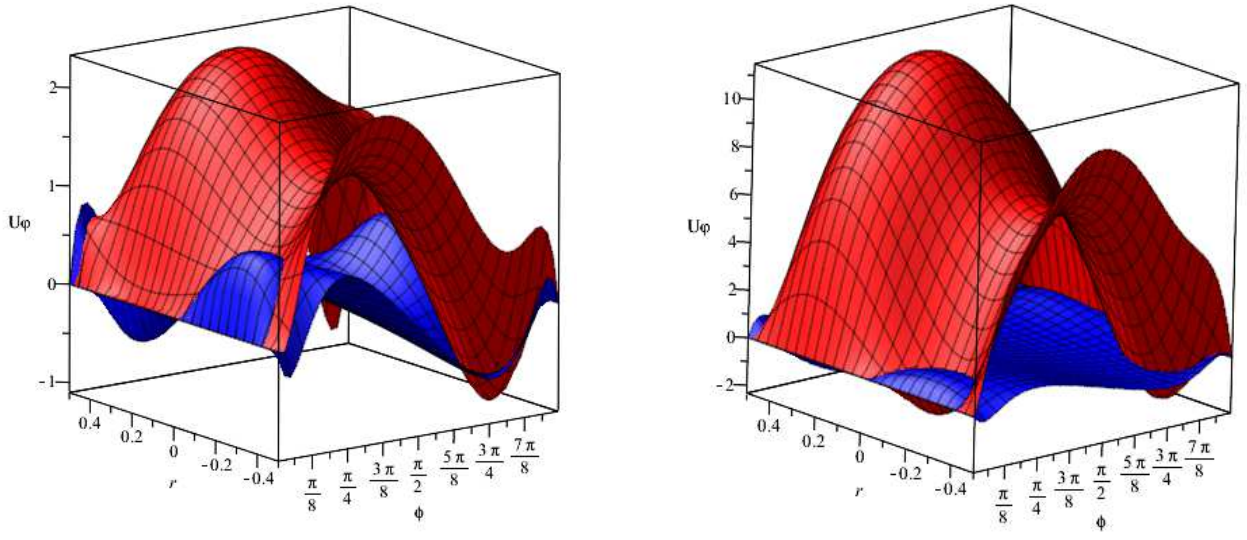

Fig. 10. Comparison between the shear layer's movement (U_φ) for (a) $q_\varphi = 0.1q_r$ (b) $q_\varphi = 0.5q_r$.

The results will be very important in terms of shifting the q_φ load in terms of shifting in the φ direction. Because q_φ is in line with φ and will directly affect U_φ. It is observed that only by considering the value of q_φ = 0.1q_r, the maximum value of U_φ is about 4 times higher than the case where q_φ is equal to zero (Fig. 10a). This increase in U_φ per q_φ = 0.5q_r will result in an approximately 10-fold increase in the maximum U_φ value (Fig. 10b). So even small values in q_φ will greatly affect the U_φ latitude shift, and ignoring it will cause serious errors. As the q_φ value increases, the results of the U_φ displacement in the r and φ directions will change. U_φ changes are not regular and are three-dimensional and irregular. Therefore, the interpretation of the obtained U_φ diagrams has its own complexity and no specific process can be considered for it. Of course, here the effects of the displacement of the Earth's inner layers on the displacement of the layers at the Earth's surface are more important. In other words, for r = h/2, which in fact represents a depth equal to zero at the Earth's surface, the criterion will be the results of displacements at the Earth's surface. If the value of r = h/2 is considered in the two introduced three-dimensional diagrams, a two-dimensional diagram of the changes w and U_φ in terms of φ angle can be obtained, and for each value of the φ angle, which actually represents the distance from the Arctic is geographic (φ = 0 North Pole, φ = π/2 equator, and φ = π Antarctica) obtain a specific value for radial w and U_φ displacements. By analyzing the values of the obtained displacements, valuable information can be obtained about the motion of the inner and surface layers of the Earth. It is even possible to make the necessary predictions about the amount of movement of the layers in a certain area by having the amount of internal pressure.

7. Conclusion

Mathematical modeling of the movement of the Earth's layers under pressure is performed in the present study. The nonlinear dynamic governing equations of Earth (which is considered the geometry of a perfect sphere) are derived based on the two-dimensional first-order shear deformation theory, as well as two quasi-three-dimensional theories proposed for modeling thick spherical structures for the first time. The extracted dynamic equations are completely nonlinear and go beyond von Kármán strain

field theory. In other words, nonlinear terms are considered in all directions and not for the direction of the applied load only. The pressure on the target layer is considered a function of the thickness of the structure, which indicates the pressure of the inner layers of the Earth from the free surface adjacent to the atmosphere to the considered area. The reason for this is that the obtained results would be more accurate. In general, the most important achievements of this research can be summarized as follows:

- Dynamic quasi-three-dimensional nonlinear simulation of the movements of the Earth's layers in different directions in the form of a system of partial differential equations is carried out in this research.
- Radial and transverse movements of the Earth's layers under internal pressures are illustrated in the form of three-dimensional diagrams in the latitude and radial (depth) directions.
- The results can provide very good information to researchers and scientists who study the movements of the Earth's inner layers in terms of predicting the tectonic movements and the occurrence of earthquakes.
- The effect of shear loads on the radial and latitude movements of the Earth's layers is investigated in this research. In other words, according to the governing equations the load can be applied in all directions.

Author Contributions

Shahriar Dastjerdi: Conceptualization, Methodology, Software, Validation, Visualization, Investigation, Writing-original draft preparation, Formal analysis; Mohammad Malikan: Methodology, Investigation, Writing-original draft preparation, Writing-review and editing, Resources; Bekir Akgöz: Methodology, Data curation, Resources; Ömer Civalek: Methodology, Project administration, Supervision; Victor Eremeyev: Methodology, Project administration, Supervision. All authors discussed the results, reviewed, and approved the final version of the manuscript.

Acknowledgments

Not applicable.

Conflict of Interest

The authors declared no potential conflicts of interest concerning the research, authorship, and publication of this article.

Funding

The authors received no financial support for the research, authorship, and publication of this article.

Data Availability Statements

The datasets generated and/or analyzed during the current study are available from the corresponding author on reasonable request.

Nomenclature

$\rho(r)$	Density [kg/m^3]	ω_E	Rotational speed of the Earth [m/S]
$g(r)$	Gravitational acceleration [m/S^2]	q_r	Pressure throughout the Earth's crust
G	Universal gravitational [m^3/kgS^2]	q_θ	Pressure in line with θ
R	Average radius of the Earth [m]	q_φ	Pressure in line with φ
E	Strain tensor	T	Matrix transpose
$\overrightarrow{\mathrm{U}}$	Displacement vector	∇	Gradient
$\hat{\mathrm{e}}_\mathrm{r}, \hat{\mathrm{e}}_\theta, \hat{\mathrm{e}}_\varphi$	The components of strain tensor	α_{Th}	Thermal expansion coefficient
r, θ, φ	Geometrical directions	ΔT	Temperature variation
U_r, U_θ, U_φ	Displacement functions	h	Thickness of Earth's crust
δ	Energy variational parameter	a_r, a_φ	Radial and lateral accelerations
$N_{rr}, N_{\varphi\varphi}, N_{\theta\theta}, N_{r\varphi}$	Axial stress resultants	U_ε, U_k	Strain and Kinetic energy
$M_{\varphi\varphi}, M_{\theta\theta}, M_{r\varphi}$	Moment stress resultants	E	Young's modulus [GPa]
$P_{\varphi\varphi}, P_{\theta\theta}$	Mathematical stress resultants	ν	Poisson's ratio
u_0, v_0, w_0	Displacements of the mid-plane [m]	σ_{ij}	Stress
ψ_1, ψ_2	Rotations of elements	ε_{ij}	Strain
r	Thickness coordinate [m]	t	Time [S]
u_i, v_i, w_i	Unknown parameters of displacements [m]	N	Convergence factor

References

[1] Navabi, M., Barati, M., Mathematical modeling and simulation of the earth's magnetic field: A comparative study of the models on the spacecraft attitude control application, *Applied Mathematical Modelling*, 46, 2017, 365-381.
[2] Xiao, S., Xia, P., Variational calculus method for passive earth pressure on rigid retaining walls with strip surcharge on backfills, *Applied Mathematical Modelling*, 83, 2020, 526-551.
[3] Alexandrov, D.V., Malygin, A.P., Mathematical modeling of solidification process near the inner core boundary of the Earth, *Applied Mathematical Modelling*, 37(22), 2013, 9368-9378.
[4] Vishwakarma, S.K., Runzhang, X., Rayleigh wave dispersion in an irregular sandy Earth's crust over orthotropic mantle, *Applied Mathematical Modelling*, 40(19-20), 2016, 8647-8659.

[5] Wang, J.M., Lanari, P., Wu, F.Y., Zhang, J.J., Khanal, G.P., Yang, L., First evidence of eclogites overprinted by ultrahigh temperature metamorphism in Everest East, Himalaya: Implications for collisional tectonics on early Earth, *Earth and Planetary Science Letters*, 558, 2021, 116760.
[6] Palin, R.M., Santosh, M., Cao, W., Li, S.S., Hernández-Uribe, D., Parsons, A., Secular change and the onset of plate tectonics on Earth, *Earth-Science Reviews*, 207, 2020, 103172.
[7] Zheng, Y.F., *Plate Tectonics*, Encyclopedia of Geology, second ed., 2021.
[8] Chattopadhyay, A., Gupta, S., Sharma, V.K., Kumari, P., Propagation of SH waves in an irregular monoclinic crustal layer, *Archive of Applied Mechanics*, 78, 2008, 989–999.
[9] Van Hunen, J., *Onset and Evolution of Plate Tectonics: Geodynamical Constraints*, Reference Module in Earth Systems and Environmental Sciences, 2019.
[10] Capitanio, F.A., Gonzalez, C.M., Brune, S., *Numerical Modeling of Tectonic Processes*, Encyclopedia of Geology, Second Ed., 2021.
[11] Pang, F.Z., Li, H.C., Wang, X.R., Miao, X.H., Li, S., A semi analytical method for the free vibration of doubly-curved shells of revolution, *Computers & Mathematics with Applications*, 75(9), 2018, 3249-3268.
[12] Dastjerdi, S., Akgöz, B., New static and dynamic analyses of macro and nano FGM plates using exact three-dimensional elasticity in thermal environment, *Composite Structures*, 192, 2018, 626-641.
[13] Dastjerdi, S., Akgöz, B., Yazdanparast, L., A new approach for bending analysis of bilayer conical graphene panels considering nonlinear van der Waals force, *Composites Part B: Engineering*, 150, 2018, 124-134.
[14] Dastjerdi, S., Lotfi, M., Jabbarzadeh, M., Nonlocal analysis of single and double-layered graphene cylindrical panels and nano-tubes under internal and external pressures considering thermal effects, *Journal of Theoretical and Applied Mechanics*, 55, 2017, 883-896.
[15] Zeighampour, H., Tadi Beni, Y., Analysis of conical shells in the framework of coupled stresses theory, *International Journal of Engineering Science*, 81, 2014, 107-122.
[16] Dastjerdi, S., Akgöz, B., On the statics of fullerene structures, *International Journal of Engineering Science*, 142, 2019, 125-144.
[17] Pietraszkiewicz, W., Refined resultant thermomechanics of shells, *International Journal of Engineering Science*, 49, 2011, 1112-1124.
[18] Gal, E., Levy, R., Geometrically nonlinear analysis of shell structures using a flat triangular shell finite element, *Archive of Computational Methods in Engineering*, 13, 2006, 331–388.
[19] Dastjerdi, S., Akgöz, B., Civalek, Ö., On the effect of viscoelasticity on behavior of gyroscopes, *International Journal of Engineering Science*, 149, 2020, 103236.
[20] Chen, Y., Avitabile, P., Page, C., Dodson, J., A polynomial based dynamic expansion and data consistency assessment and modification for cylindrical shell structures, *Mechanical Systems and Signal Processing*, 154, 2021, 107574.
[21] Jiang, B., Zhang, J., Ohsaki, M., Shape optimization of free-form shell structures combining static and dynamic behaviors, *Structures*, 29, 2021, 1791-1807.
[22] Lavrencic, M., Brank, B., Hybrid-Mixed Low-Order Finite Elements for Geometrically Exact Shell Models: Overview and Comparison, *Archives of Computational Methods in Engineering*, 28, 2021, 3917–3951.
[23] Lee, C.Y., Hodges, D.H., Hybrid energy transformation to generalized Reissner–Mindlin model for laminated composite shells, *International Journal of Engineering Science*, 122, 2018, 30-55.
[24] Zhang, Z., Zhou, W., Gao, S., Wan, M., Zhang, W., A novel computational method for dynamic analysis of flexible sandwich plates undergoing large deformation, *Archive of Applied Mechanics*, 91, 2021, 4069–4080.
[25] Li, J., Ren, H., Ning, J., Deformation and failure of thin spherical shells under dynamic impact loading: Experiment and analytical model, *Thin-Walled Structures*, 161, 2021, 107403.
[26] Sharma, N., Panda, S.K., Multiphysical numerical (FE-BE) solution of sound radiation responses of laminated sandwich shell panel including curvature effect, *Computers & Mathematics with Applications*, 80(5), 2020, 1221-1239.
[27] Eyvazian, A., Shahsavari, D., Karami, B., On the dynamic of graphene reinforced nanocomposite cylindrical shells subjected to a moving harmonic load, *International Journal of Engineering Science*, 154, 2020, 103339.
[28] Fadida, R., Shirizly, A., Rittel, D., The static and dynamic shear-tension mechanical response of AM Ti6Al4V containing spherical and prolate voids, *International Journal of Engineering Science*, 141, 2019, 1-15.
[29] Serhat, G., Anamagh, M.R., Bediz, B., Basdogan, I., Dynamic analysis of doubly curved composite panels using lamination parameters and spectral-Tchebychev method, *Computers & Structures*, 239, 2020, 106294.
[30] Li, G., Su, X., Pu, H., An unconditionally stable and high-accuracy finite element scheme for dynamic analysis of saturated poroelastic media, *Soil Dynamics and Earthquake Engineering,* 136, 2020, 106226.
[31] Viana, H.F., da Silva, R.G.L., Costa, R.S., Lavall, A.C.C., Formulation for nonlinear dynamic analysis of steel frames considering the plastic zone method, *Engineering Structures*, 223, 2020, 111197.
[32] Huang, Y., Sturt, R., Willford, M., A damping model for nonlinear dynamic analysis providing uniform damping over a frequency range, *Computers & Structures*, 212, 2019, 101-109.
[33] Li, Z.M., Liu, T., Qiao, P., Nonlinear vibration and dynamic instability analyses of laminated doubly curved panels in thermal environments, *Composite Structures*, 267, 2020, 113434.
[34] Fu, T., Wu, X., Xiao, Z., Chen, Z., Dynamic instability analysis of porous FGM conical shells subjected to parametric excitation in thermal environment within FSDT, *Thin-Walled Structures*, 158, 2021, 107202.
[35] Zhang, H., Zhu, X., Yao, S., Nonlinear dynamic analysis method for large-scale single-layer lattice domes with uncertain-but-bounded parameters, *Engineering Structures*, 203, 2020, 109780.
[36] Hashemian, M., Falsafioon, M., Pirmoradian, M., Toghraie, D., Nonlocal dynamic stability analysis of a Timoshenko nanobeam subjected to a sequence of moving nanoparticles considering surface effects, *Mechanics of Materials*, 148, 2020, 103452.
[37] Ramirez, D., Cuba, L., Mantari, J.L., Arciniega, R.A., Bending and Free Vibration Analysis of Functionally Graded Plates via Optimized Non-polynomial Higher Order Theories, *Journal of Applied and Computational Mechanics*, 5(2), 2019, 281–298.
[38] Chen, X., Gan, X., Ren, G., Dynamic modeling and nonlinear analysis of a rotor system supported by squeeze film damper with variable static eccentricity under aircraft turning maneuver, *Journal of Sound and Vibration*, 485, 2020, 115551.
[39] Kuppa, S.K., Lal, M., Dynamic behaviour analysis of coupled rotor active magnetic bearing system in the supercritical frequency range, *Mechanism and Machine Theory,* 152, 2020, 103915.
[40] Su, W., Qiu, Y.X., Xu, Y.J., Wang, J.T., A scheme for switching boundary condition types in the integral static-dynamic analysis of soil-structures in Abaqus, *Soil Dynamics and Earthquake Engineering,* 141, 2021, 106458.
[41] Arruda, M.R.T., Castro, L.M.S., Non-linear dynamic analysis of reinforced concrete structures with hybrid mixed stress finite elements, *Advances in Engineering Software*, 153, 2021, 102965.
[42] Sahoo, R., Grover, N., Singh, B.N., Random vibration response of composite–sandwich laminates, *Archive of Applied Mechanics*, 91, 2021, 3755–3771.
[43] Monge, J.C., Mantari, J.L., Yarasca, J., Arciniega, R.A., On Bending Response of Doubly Curved Laminated Composite Shells Using Hybrid Refined Models, *Journal of Applied and Computational Mechanics,* 5(5), 2019, 875-899.
[44] Mellouli, H., Jrad, H., Wali, M., Dammak, F., Free vibration analysis of FG-CNTRC shell structures using the meshfree radial point interpolation method, *Computers & Mathematics with Applications*, 79(11), 2020, 3160-3178.
[45] Zhao, Z., Yuan, X., Zhang, W., Niu, D., Zhang, H., Dynamical modeling and analysis of hyperelastic spherical shells under dynamic loads and structural damping, *Applied Mathematical Modelling*, 95, 2021, 468-483.
[46] Xie, J., Hao, S., Wang, W., Shi, P., Analytical solution of stress in functionally graded cylindrical/spherical pressure vessel, *Archive of Applied Mechanics*, 91, 2021, 3341–3363.
[47] Yi, H., Sahmani, S., Safaei, B., On size-dependent large-amplitude free oscillations of FGPM nanoshells incorporating vibrational mode interactions, *Archives of Civil and Mechanical Engineering*, 20, 2020, 48.
[48] Ameijeiras, M.P., Godoy, L.A., Quasi-bifurcation and Imperfection-sensitivity of Cylindrical Shells under Pressures due to an Explosion, *Journal of Applied and Computational Mechanics,* 7(2), 2021, 984-992.
[49] Abouelregal, A.E., Mohammad-Sedighi, H., Faghidian, S.A., Shirazi, A.H., Temperature-dependent physical characteristics of the rotating nonlocal nanobeams subject to a varying heat source and a dynamic load, *Facta Universitatis, Series: Mechanical Engineering*, 19(4), 2021, 633-56.
[50] Fattahi, A.M., Safaei, B., Qin Zh., Chu, F., Experimental studies on elastic properties of high density polyethylene-multi walled carbon nanotube nanocomposites, *Steel and Composite Structures*, 38(2), 2021, 177-187.
[51] Ghanati, P., Safaei, B., Elastic buckling analysis of polygonal thin sheets under compression, *Indian Journal of Physics*, 93, 2019, 47–52.

[52] Safaei, B., Frequency-dependent damped vibrations of multifunctional foam plates sandwiched and integrated by composite faces, *The European Physical Journal Plus*, 136, 2021, 646.
[53] Safaei, B., The effect of embedding a porous core on the free vibration behavior of laminated composite plates, *Steel and Composite Structures*, 35(5), 2020, 659-670.
[54] Fragassa, C., de Camargo, F. V., Pavlovic, A., Minak, G., Explicit numerical modeling assessment of basalt reinforced composites for low-velocity impact, *Composites Part B: Engineering*, 163, 2019, 522-535.
[55] Fragassa, C., de Camargo, F. V., Pavlovic, A., Minak, G., Experimental evaluation of static and dynamic properties of low styrene emission vinylester laminates reinforced by natural fibres, *Polymer Testing*, 69, 2018, 437-449.
[56] Pavlovic, A., Fragassa, C., Numerical modelling of ballistic impacts on flexible protection curtains used as safety protection in woodworking, *Proceedings of the Institution of Mechanical Engineers, Part C: Journal of Mechanical Engineering Science*, 231(1), 2017, 44-58.
[57] Malikan, M., Eremeyev, V.A., On dynamic modeling of piezomagnetic/flexomagnetic microstructures based on Lord–Shulman thermoelastic model, *Archive of Applied Mechanics*, (2022). https://doi.org/10.1007/s00419-022-02149-7
[58] Malikan, M., Eremeyev, V.A., On a flexomagnetic behavior of composite structures, *International Journal of Engineering Science*, 175, 2022, 103671.
[59] Malikan, M., Krasheninnikov, M., Eremeyev, V.A., Torsional stability capacity of a nano-composite shell based on a nonlocal strain gradient shell model under a three-dimensional magnetic field, *International Journal of Engineering Science*, 148, 2020, 103210.
[60] Gutenberg, B., Density, Pressure, Gravity, and Flattening in the Earth, *International Geophysics*, 1, 1959, 149-164.
[61] Kennett, B.L.N., On the density distribution within the Earth, *Geophysical Journal International*, 132(2), 1998, 374-382.
[62] Dastjerdi, Sh., Malikan, M., Akgöz, B., Civalek, Ö., Wiczenbach, T., Eremeyev, V.A., On the deformation and frequency analyses of SARS-CoV-2 at nanoscale, *International Journal of Engineering Science*, 170, 2022, 103604.
[63] Gutenberg, B., Elastic Constants, and Elastic Processes in the Earth, *International Geophysics*, 1, 1959, 165-184.
[64] Speziale, S., *Elastic properties of Earth materials*, Conference: From Core to Crust: Towards an Integrated Vision of Earth's Interior, Miramare, Trieste, Italy, 2009.
[65] Anderson, D.L., *Theory of the Earth*, Blackwell Scientific Publications, Boston, MA, 1989.
[66] Dastjerdi, S., Tadi Beni, Y., Malikan, M., A comprehensive study on nonlinear hygro-thermo-mechanical analysis of thick functionally graded porous rotating disk based on two quasi-three-dimensional theories, *Mechanics Based Design of Structures and Machines*, 50(10), 2020, 3596-3625.
[67] Dastjerdi, S., Malikan, M., Dimitri, R., Tornabene, F., Nonlocal elasticity analysis of moderately thick porous functionally graded plates in a hygro-thermal environment, *Composite Structures*, 255, 2021, 112925.

ORCID iD

Shahriar Dastjerdi https://orcid.org/0000-0003-4256-240X
Mohammad Malikan https://orcid.org/0000-0001-7356-2168
Bekir Akgöz https://orcid.org/0000-0003-2097-2555
Ömer Civalek https://orcid.org/0000-0003-1907-9479
Victor A. Eremeyev https://orcid.org/0000-0002-8128-3262

How to cite this article: Dastjerdi Sh., Malikan M., Akgöz B., Civalek Ö., Eremeyev V.A. A novel approach to fully nonlinear mathematical modeling of tectonic plates, *J. Appl. Comput. Mech.*, xx(x), 2023, 1–15. https://doi.org/10.22055/jacm.2022.41704.3800